FUNDAMENTAL POWER COUPLER DEVELOPMENT FOR LOW-BETA SUPERCONDUCTING CAVITIES

By

Jon Joseph Wlodarczak

A THESIS

Submitted to
Michigan State University
in partial fulfillment of the requirements
for the degree of

MASTER OF SCIENCE

Electrical and Computer Engineering

2008

UMI Number: 1463062

INFORMATION TO USERS

The quality of this reproduction is dependent upon the quality of the copy submitted. Broken or indistinct print, colored or poor quality illustrations and photographs, print bleed-through, substandard margins, and improper alignment can adversely affect reproduction.

In the unlikely event that the author did not send a complete manuscript and there are missing pages, these will be noted. Also, if unauthorized copyright material had to be removed, a note will indicate the deletion.

UMI®

UMI Microform 1463062

Copyright 2009 by ProQuest LLC.

All rights reserved. This microform edition is protected against unauthorized copying under Title 17, United States Code.

ProQuest LLC
789 E. Eisenhower Parkway
PO Box 1346
Ann Arbor, MI 48106-1346

ABSTRACT

FUNDAMENTAL POWER COUPLER DEVELOPMENT FOR LOW-BETA SUPERCONDUCTING CAVITIES

By

Jon Joseph Wlodarczak

The construction of a re-accelerator for secondary ion beams is currently underway at the National Superconducting Cyclotron Laboratory (NSCL). This re-accelerating linear accelerator (linac) will use superconducting quarter-wave resonators operating at 80.5 MHz with $\beta = 0.041$ and $\beta = 0.085$, where β is the velocity of a particle relative to the speed of light. Input coupling will be done using a coaxial probe-type radio frequency (RF) fundamental power coupler (FPC) for both quarter-wave resonator (QWR) cavities. Custom-designed power couplers are expensive, complicated, and can have long lead times. The FPCs presented in this thesis will be operated with fixed coupling, using continuous wave (CW) input power operating at a maximum of 1 kW. The key component of the coupler is a commercially-available RF feedthrough to reduce the cost and production time. This feedthrough allows the cavity to maintain a clean vacuum with pressure less than 1×10^{-8} torr. Another concern is the heat leak to the cryomodule's cold mass at 4.5 K. The design goal for each coupler is to produce less than 1 W of static heat load to the cold mass.

Four prototype FPCs were fabricated. Two of the FPCs were assembled back-to-back, pumped out, and conditioned with both traveling wave and standing wave power using a 1 kW RF amplifier. Experience with the prototype FPCs provided the basis for the design of production FPCs for the re-accelerator.

For Fred

ACKNOWLEDGMENT

This thesis would have never been possible without the help of many people. First I would like to thank my advisors Dr. Leo Kempel and Dr. Walter Hartung for providing me the opportunity to work on this project. Their collective guidance was immeasurable. Thanks are also in order to the professors and students in the electromagnetics group at MSU. They provided me with the knowledge to make it through.

I would also like to thank everyone at the National Superconducting Cyclotron Laboratory for having me as part of their team. I would especially like to thank Jim Wagner and Kurt Kranz for getting my foot in the door as an undergraduate. Working with the SRF group has given me the support and equipment which enabled me to work on this project. Without the technical knowledge of John Popielarski, I would not have been able to accomplish as much. I would also like to thank David Norton for all of his work with the data acquisition during conditioning, Laura Popielarski for her clean room assistance, Patrick Glennon for his mechanical design work, Matt Johnson for his work with ANSYS, Steve Bricker, John Bierwagen, and everybody else that provided assistance.

Most of all I would like to thank my wife for supporting me throughout this entire process, both financially and emotionally. Without her, I would never have gotten to where I am today. This is for Danielle.

TABLE OF CONTENTS

LIST OF TABLES

LIST OF FIGURES

KEY TO ABBREVIATIONS

NSCL: National Superconducting Cyclotron Laboratory

MSU: Michigan State University

ReA3: Re-Accelerator, 3 MeV

LINAC: Linear Accelerator

RIBs: Rare Isotope Beams

RIA: Rare Isotope Accelerator

FRIB: Facility for Rare Isotope Beams

QWR: Quarter Wave Resonator

RF: Radio Frequency

FPC: Fundamental Power Coupler

SRF: Superconducting Radio Frequency

CW: Continuous Wave

VNA: Vector Network Analyzer

RRR: Residual Resistance Ratio

RFQ: Radio Frequency Quadrupole

HOM: Higher Order Mode

OFHC: Oxygen-Free High Conductivity

IR: Infrared

CF: ConFlat

RGA: Residual Gas Analyzer

KEY TO SYMBOLS

a: Diameter of inner conductor [m]

$A, A_{ss}, A_{cu}, A_{ic}, A_{oc}$: Cross-sectional area [$m^2$]

b: Diameter of outer conductor [m]

B_{pk}: Peak magnetic field [T]

B_ϕ: Magnetic flux density, azimuthal [T]

BW: Bandwidth [Hz]

c: Speed of light [2.998×10^8 m/s]

c: Diameter of dielectric liner [m]

d: Width of rectangular waveguide [m]

E_{acc}: Accelerating (electric) field [V/m]

E_{pk}: Peak electric field [V/m]

E_r: Electric field, radial [V/m]

f_o: Resonant frequency [Hz]

G: Geometry Factor [Ω]

H: Magnetic field intensity [A/m]

I_o: Peak current [A]

$k(T)_{ss}, k(T)_{cu},$: Temperature dependent thermal conductivity [W/(mK)]

L: Gap length [m]

L_{min}: Minimum coupler length [inches]

P_{beam}: Beam power [W]

P_c: Power dissipated in a cavity [W]

P_{ext}: Transient power emitted from a cavity [W]

P_{fwd}: Forward power [dBm]

P_g: Power supplied by RF generator [W]

P_p: Power dissipated through pick-up coupler [W]

P_r: Reflected power [W]

P_{sw}: Standing wave equivalent power [dBm]

P_t: Transmitted power [W]

q_{cond}: Conducted heat transfer [W]

q_{rad}: Radiated heat transfer [W]

q_{RF}: RF conduction heat transfer [W]

q_{total}: Total heat transfer [W]

Q_{ext}: External quality factor

Q_L: Loaded quality factor

Q_o: Intrinsic quality factor

Q_{stat}: Static heat leak [W]

Q_{tot}: Total heat leak [W]

R_L: Load resistance [Ω]

R_s: Surface resistance [Ω]

t_{ss}: Wall thickness of stainless steel [inches]

t_{cu}: Copper plating thickness [# of skin depths]

U: Stored energy in a cavity [J]

V_{acc}: Accelerating voltage [V]

V_p: Peak voltage [V]

Z_g: Impedance of partially-filled transmission line [Ω]

Z_o: Characteristic impedance of a transmission line [Ω]

β: Relative velocity

β_{ext}: Coupling factor

$\beta_{ext,p}$: Pick-up coupling factor

$\beta_{ext,t}$: Input coupling factor

Γ_L: Reflection coeffecient of coupler transmission line

Γ_w: Reflection coeffecient of coupler window

δ: Skin depth [m]

ε_o: Permittivity of free space $[1/\mathfrak{c}^2\mu_o = 8.8541878 \times 10^{-12}$ F/m]

$\varepsilon_1, \varepsilon_2$: Relative permittivity of a dielectric

ϵ: Emissivity

η_o: Intrinsic impedance of free-space [Ω]

λ: Wavelength [m]

λ_c: Cut-off wavelength [m]

μ_o: Permeability of free space $[4\pi \times 10^{-7}$ N/A^2]

ρ: Electrical resistivity [Ωm]

σ: Electrical conductivity [$(\Omega\text{m})^{-1}$]

σ_{SB}: Stefan-Boltzmann constant $[5.6703 \times 10^{-8}$ W/m^{2}K^4]

ω: Angular frequency [radians/sec.]

Chapter 1

Introduction

A particle accelerator is a device which is used to accelerate charged particles to high velocities using electric fields. These high speed particles are then collided with a target to create new nuclei. This is why particle accelerators are sometimes called "atom smashers." These new isotopes do not normally exist on Earth, and last for only minute fractions of a second. Measuring the properties of these rare isotopes helps researchers begin to understand how an element is formed, or what holds a nucleus together. These answers can begin to unravel the origin of elements, or even why stars shine. Particle accelerators also have applications in archeology, national security, and medicine.

The National Superconducting Cyclotron Laboratory (NSCL) is a world leader in the research of rare isotopes. Located on the campus of Michigan State University (MSU), NSCL operates two coupled superconducting cyclotrons. Beams are injected into the K500 cyclotron then sent to the K1200 cyclotron for additional acceleration [1]. Together, these two cyclotrons can accelerate particles up to 200 MeV per nucleon. NSCL has also built the first superconducting cyclotron for medicine, the K100 Neutron Therapy Cyclotron at Harper-Grace Hospital in Detroit [2].

NSCL will be the first facility in the world to demonstrate the ability to create, stop and re-accelerate exotic beams. A conceptual diagram of the system, currently

titled ReA3, is shown in Figure 1.1 [3]. The construction of ReA3 to re-accelerate these secondary ion beams is currently underway.

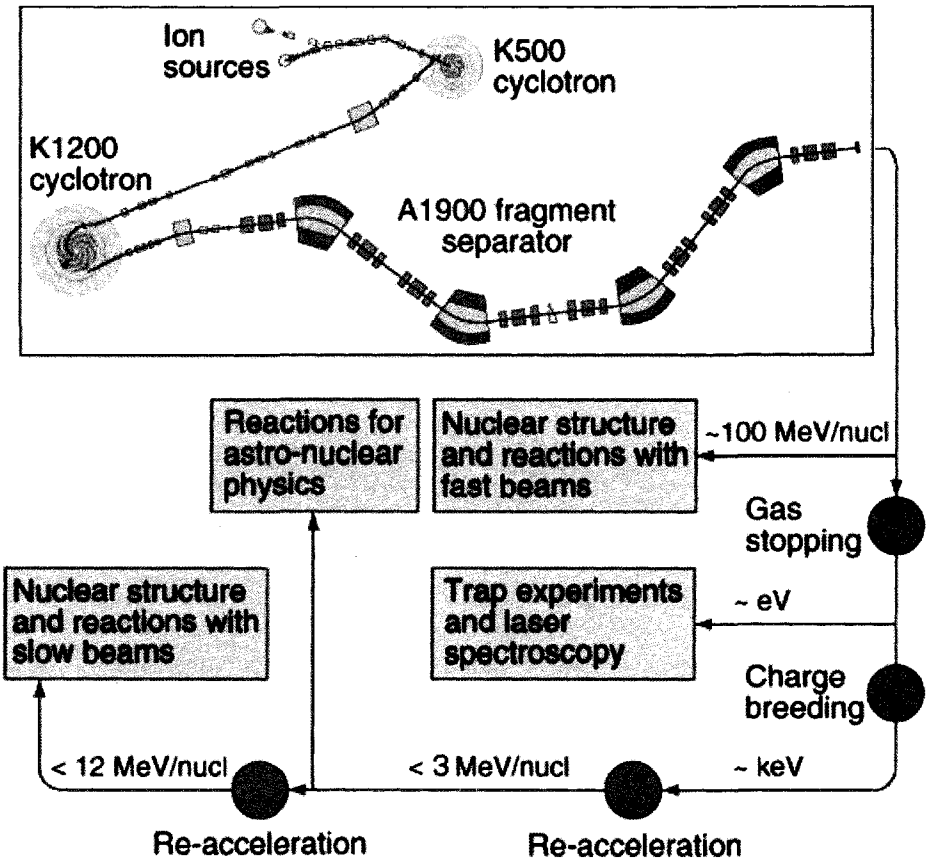

Figure 1.1: A conceptual view of the NSCL gas stopper and re-accelerator.

Linear accelerators (linacs) are able to accelerate particles to much higher energies than circular accelerators. This is due to synchrotron radiation which is created as the particles accelerate around the center. The radiation energy lost by the particle beam must be restored by the accelerator. This limits the amount of energy that can be transferred to the beam.

Using the cyclotron as an injector for ReA3, rare isotope beams (RIBs) can be accelerated at a lower cost than a dedicated facility, such as the Rare Isotope Accelerator (RIA) [4], or the Facility for Rare Isotope Beams (FRIB). The cavity designs of ReA3 are the same as those already developed and tested for RIA, requiring less

development time and cost.

ReA3 will utilize three cryomodules, containing a total of fifteen 80.5 MHz quarter-wave resonator (QWR) cavities. The modules will also contain eight superconducting solenoid magnets to be used for focusing [5]. A cryomodule is a complex component of the linac that contains liquid helium and operates at temperatures as low as 2 K. The module contains the accelerator cavities, focusing elements, as well as well as the tuners and shielding necessary for particle acceleration [6].

The re-acceleration of the beams will rely heavily on low velocity QWR cavities operating at 80.5 MHz. The QWR cavities that will be used are $\beta = v/\mathfrak{c} = 0.041$ [7] and $\beta = 0.085$ [8], each requiring less than 1 kW of operating power from the radio frequency (RF) generation system.

In addition to the internal elements, the cryomodule also supports the necessary auxiliary components necessary for operation. This includes vacuum pumps, tuning actuators, gas analyzers and fundamental power couplers (FPCs). The FPC is very important to the operation of a superconducting cryomodule; it is used to transport the RF power from the generation system into the cryomodule, and to the cavity. There are many approaches used to couple power into cavities [9, 10]. Power couplers can be quite complicated, and requires the cooperation of several engineering disciplines. This makes the design of the coupler one of the key areas of research in superconducting RF (SRF) development of accelerating cavities.

A prototype cryomodule has been constructed at NSCL to measure the performance of the QWR cavities and FPCs initially designed for RIA [11]. This module utilizes a coaxial coupler originally designed by Moblo [12]. Using information gathered during the testing of the module, a new prototype power coupler has been designed. The existing design has a small diameter inner conductor and thin ceramic window. These flaws make it susceptible to breakage during assembly. The new FPC design was optimized for continuous wave (CW) operation up to 1 kW of input power at 80.5

MHz. The FPC has fixed coupling utilizing a semi-custom vacuum feedthrough from industry. The addition of a larger center conductor, thicker alumina, and less obtrusive air-side geometry will increase durability. This feedthrough allowed the design to remain affordable, and yet be robust enough to handle the power requirements of the NSCL re-accelerator project. Additionally, coupler diagnostic ports have been added to monitor the condition of the window, a feature that was not included previously. Most commercially built input couplers are designed for much higher power applications, and are quite expensive because of this. Typically the cost of manufacturing a coupler is very high, in the tens of thousands of dollars [13]. This is close to the cost of the cavities themselves. Additionally, the range and type of superconducting accelerators is so varied, there is no one coupler that fits all applications [14].

This thesis will discuss the continuing development of an affordable FPC for NSCL. A brief introduction to superconducting cavities and linear accelerator concepts will be provided in Chapter 2. Additionally, Chapter 2 will present the parameters and specifications for the cavities that the couplers will be used to excite.

A more detailed analysis of coupler design is presented in Chapter 3. This includes background on the various methods used to get power in and out of a cavity, and coupler placement. In addition, common problem areas will be addressed.

Chapter 4 discusses the design considerations that were used in the development of the couplers. This includes both electrical and mechanical analysis. The diagnostic methods used to minimize the most common design issues will also be described.

In Chapter 5, an overview of the processes used during the conditioning of the prototype assemblies will be presented, including the procedures and the equipment used. Also provided in Chapter 5 are the results of conditioning. This chapter will discuss the outcome of the conditioning in addition to addressing issues that arose during conditioning, such as problems that developed in the design, assembly, and testing of the prototypes.

Chapter 6 is the conclusion to this thesis. A summary of the findings and results will be presented. Recommendations for adjusting the conditioning procedures as well as considerations for future work on the FPC will be provided.

Chapter 2

Superconducting Cavities and Linear Accelerators

The re-accelerator project at NSCL relies heavily on superconducting cavities. These SRF cavities provide greater accelerating capabilities than their normal conducting counterparts. Trade-offs include increased initial costs in materials and facilities, with gains in accelerating gradient and reduced RF generation costs. An introduction to SRF cavities is given in Section 2.1. Section 2.2 provides further detail on the QWR cavities that will be used in the re-accelerator. Finally, Section 2.3 explains the application of the cavities for the acceleration of exotic beams, and future acceleration projects at MSU.

2.1 Superconducting Cavities

The primary function of a resonant cavity is to impart energy to a beam of charged particles using a time-varying electric field. The TM_{010} mode is commonly chosen for operation of pillbox cavities operating in π mode, because it is the lowest order mode that has an electric field along the beam axis, which is what provides acceleration. Coaxial resonators use a TEM mode to create the accelerating field. Magnetic fields

do not add energy to the beam, however they are useful for focusing. Focusing is done elsewhere in the linac using superconducting solenoids.

Superconductivity is desirable because it allows large accelerating fields to be generated without a large amount of power loss in the cavity walls. Much of the losses occur due to surface resistance. Normal conducting copper cavities have surface resistance on the order of 10^{-3} Ω, depending on the frequency and temperature. In comparison the typical surface resistance of superconducting niobium cavities range from 10 to 100 $n\Omega$ [15].

These losses within the cavity can be described by the quality factor Q_o, or the intrinsic Q of the cavity. The quality factor is a figure of merit for resonant cavities; it is a measure of the number of RF cycles that a cavity will go through before it dissipates the energy stored within. The quality factor is expressed as

$$Q_o = \omega \frac{Energy\ Stored\ in\ Cavity}{Power\ Dissipated\ in\ Cavity} = \frac{\omega U}{P_c} \tag{2.1}$$

The quality factor can also be written as

$$Q_o = \frac{G}{R_s} \tag{2.2}$$

where R_s is the surface resistance and G is the geometry factor:

$$G = \frac{\omega \mu_o \int_V |\mathbf{H}|^2 \, dv}{\int_S |\mathbf{H}|^2 \, ds} \tag{2.3}$$

It is easily seen from Equation (2.2) that the quality factor of a superconducting cavity is approximately five orders of magnitude higher than that of copper because of the reduced surface resistance. The geometry factor depends on the shape of the cavity, not its size or material, so it is convenient to use when comparing different cavity configurations.

The intrinsic Q of the cavity is useful for finding the losses in a cavity, but this is not the only mechanism for losses to occur. Additional energy can be lost through the input and pick-up couplers. Another useful term is the external quality factor, or Q_{ext}. The Q_{ext} quantifies how much energy leaks out of a port in cavity and is lost. Assuming a port terminated with an external load, we define

$$Q_{ext} = \omega \frac{Energy\ Stored\ in\ Cavity}{Power\ Dissipated\ in\ the\ External\ Load} = \frac{\omega U}{P_{ext}} \tag{2.4}$$

We can now use the above definitions to describe the total loss in the cavity, or average power dissipated. This is the loaded Q and is what can be measured using a vector network analyzer (VNA). The loaded quality factor is

$$Q_L = \omega \frac{Energy\ Stored\ in\ Cavity}{Total\ Power\ Dissipated} = \frac{\omega U}{P_T} \tag{2.5}$$

where $P_T = P_c + P_{ext}$ is the total power dissipated. For a one-port system, the relationship between the Q factors can be expressed as

$$\frac{1}{Q_L} = \frac{1}{Q_o} + \frac{1}{Q_{ext}} \tag{2.6}$$

Once the cavity is designed and built, Q_{ext} is the only quality factor than can be readily adjusted. The external Q depends on the coupling between the power generator and the cavity. This coupling factor is a measure of the coupling strength to the cavity, and is referred to as β_{ext} and defined as [1]

$$\beta_{ext} \equiv \frac{P_{ext}}{P_c} = \frac{Q_o}{Q_{ext}} \tag{2.7}$$

P_{ext} is the power emitted from the cavity to the input coupler, under a transient

[1] The 'ext' subscript will be used to differentiate the coupling factor from the normalized beam velocity (β), which is unrelated.

condition. A more detailed explanation is available in [15]. If $\beta_{ext} < 1$ the coupler and cavity are considered undercoupled. When $\beta_{ext} > 1$ the combination is considered overcoupled. When $\beta_{ext} = 1$ the cavity and coupler are considered critically coupled, or matched. When this happens, $Q_{ext} = Q_o$ and $Q_L = Q_o/2$.

Substituting Equation (2.7) into Equation (2.6) gives

$$Q_o = Q_L(1 + \beta_{ext}) \tag{2.8}$$

In the case of two couplers, one to input the power ($\beta_{ext,g}$), and a second used as a pick up ($\beta_{ext,p}$), Equation (2.8) becomes

$$Q_o = Q_L(1 + \beta_{ext,g} + \beta_{ext,p}) \tag{2.9}$$

The coupling factor of the second port can be expressed as

$$\beta_{ext,p} = \frac{P_p}{P_c} \tag{2.10}$$

where P_p is the power lost to the pick-up coupler.

There are many more important formulas pertaining to cavities, the above provide the information needed to design a power coupler. A more in-depth analysis on cavity design and performance can be found in the text by Padamsee [15].

2.2 Coaxial Quarter-Wave Resonators

ReA3 will rely on a total of sixteen QWR cavities of $\beta = 0.041$ and $\beta = 0.085$ operating at 80.5 MHz. These cavities consist of a single inner conductor, or loading element, that is $\lambda/4$ long, centered in a cylindrical outer conductor. The conductor walls are formed from niobium sheets 2 mm thick, with $RRR \geq 250$ [8]. This residual resistance ratio (RRR) is a measure of the purity of a metal. The RRR can be

formally defined as

$$RRR = \frac{Resistivity\ at\ 300\ K}{Residual\ Resistivity\ at\ Low\ Temperature\ (Normal\ Conducting)} \tag{2.11}$$

The larger the RRR, the more pure the metal is considered, up to the theoretical limit of $35,000$ [15, 16].

It has already been shown that β is the velocity of a particle relative to the speed of light. The product $\beta\lambda$ is the distance a particle of velocity β travels in a single RF period. In order to provided a positive field in each gap, cavities are designed with an inter-gap spacing of $\beta\lambda/2$. Because β is small, a lower frequency allows for a larger gap, which is more useful for acceleration [15]. However, this low frequency requires rather large cavity dimensions, which is why QWRs are chosen over other cavity types. Cavities with $\beta < 0.2$ typically have operating frequencies between 50 and 200 MHz.

The accelerating field (E_{acc}) of a cavity is given by

$$E_{acc} = \frac{V_p}{L} \tag{2.12}$$

where V_p is the peak voltage and L is the distance over which the beam experiences electric field during acceleration. Care must be taken when defining this distance, as the definition may vary between institutions. The superconducting cavities that will be used for ReA3 are shown in Figure 2.1, and the cavity parameters are provided in Table 2.1 [17, 18].

A quarter-wave cavity is a modification of a simple coaxial resonator. A coaxial resonator is formed by placing conducting end walls onto a simple coaxial transmission line. The enclosed length allows standing-wave TEM modes to exist, which have only transverse fields. In his text, Wangler [19] provides the following three formulas for

coaxial resonators:

$$B_\theta = \frac{\mu_o I_o}{\pi r} \cos(p\pi z/l) e^{j\omega t} \tag{2.13}$$

and

$$E_r = -2j\sqrt{\frac{\mu_o}{\epsilon_o}} \frac{I_o}{2\pi r} \sin(p\pi z/l) e^{j\omega t} \tag{2.14}$$

where $p = 1, 2, 3, \ldots$, $\omega = p\pi z/l$, $l = p\lambda/2$ and z is the position along the cavity, from 0 to l. The quality factor of the coaxial cavity can be expressed as

$$Q_o = \frac{p\pi}{R_s}\sqrt{\frac{\mu_o}{\epsilon_o}} \frac{\ln\left(\frac{b}{a}\right)}{\left[l\left(\frac{1}{a}+\frac{1}{b}\right) + 4\ln\left(\frac{b}{a}\right)\right]} \tag{2.15}$$

where a and b are the inner and outer conductor diameters respectively. The lowest order mode is $p = 1$ which corresponds to a half-wave resonator. A modification of the half-wave coaxial resonator is the quarter-wave. This is made by shorting one end of the center conductor, and leaving a gap at the opposite end, creating a capacitance. Beam holes are placed near the end gap, where the electric field is the greatest; these fields will be discussed further in Section 3.2.

2.3 Linacs and Re-accelerators

One would assume that the term linear accelerator would refer to any device that accelerates particles in a straight line. In fact, linac refers to an accelerator that accelerates a charged particle in a linear path using electromagnetic fields [19]. Other paths of resonant RF accelerators are spiral for a cyclotron, or circular for a synchrotron. One benefit of straight-line trajectory is that a linac provides beams of high energy and quality without the power losses caused by synchrotron radiation, which is present in circular accelerators. An advantage that cyclic accelerators offer is continuous acceleration of a particle as it circles. Another advantage is that circular accelerators take up much less space than a linac of comparable power.

ReA3 will consist of a normal conducting radio frequency quadrupole (RFQ) connected in series with three superconducting cryomodules containing a total of fifteen QWR cavities [18]. The particles being accelerated will first pass through the RFQ and then into two modules containing $\beta = 0.041$ cavities, then through one module containing $\beta = 0.085$ cavities. The beam velocity range that the cavity can efficiently accelerate is the cavity's velocity acceptance, and the range of the re-accelerator will be from $v = 0.05c$ to $v = 0.15c$; providing energies up to 3.0 MeV. A fourth module near the end of the accelerator will contain a single $\beta = 0.041$ QWR cavity and will be used as a beam rebuncher.

The size of a linac can range from a few meters to several kilometers in length, and the costs can range from a few million to a billion dollars. Both the length and cost depend on the desired final energy. The information provided here just scratches the surface on linacs and their applications. A much more detailed history and explanation can be found in the text by Wangler [19].

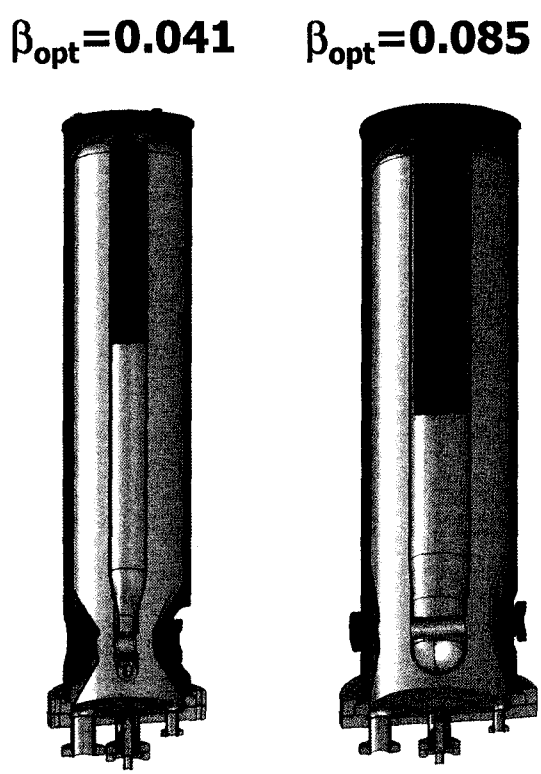

Figure 2.1: Superconducting QWRs to be used for the re-accelerator. The niobium inner and outer conductors are shown in gray, and the titanium helium vessels are shown in green.

Table 2.1: Low beta QWR cavity parameters.

Cavity Type	$\lambda/4$	$\lambda/4$
Optimum β (β_{opt})	0.041	0.085
Resonant frequency (MHz)	80.5	80.5
Number of cavities	8	8
E_{pk} (MV/m)	16.5	20
B_{pk} (mT)	28.2	49.5
V_{acc} (MV)	0.46	1.18
L (m)	0.095	0.21
E_{acc} (MV/m)	4.84	5.62
Operating Temperature (K)	4.5	4.5
$G(\Omega)$	15.7	19
$U(J)$	0.99	6.69
Q_o	5×10^8	5×10^8
Q_L	1.4×10^6	3.2×10^6
P_g (W)	236	700
P_{beam} (W)	118	350

Chapter 3

RF Power Coupling and Couplers

There are many systems necessary to successfully operate a superconducting cavity. Perhaps none are more critical than the fundamental power coupler. Without the FPC supplying RF power to the cavity, there would be no electric field to accelerate the beam. If a coupler fails, it can disable the cavity or even the entire accelerator.

Section 3.1 provides a brief introduction to the three most common types of power couplers. FPC location and style considerations are discussed in Section 3.2. The function and design analysis of the RF window are given in Section 3.3. Material constraints and analysis of heat load are given in Section 3.4. Conductor sizing and matching are presented in Section 3.5. Section 3.6 explains how the desired coupling strength (Q_{ext}) is determined. Lastly, Section 3.7 introduces various faults and the consequences of a coupler failure.

3.1 Fundamental Power Couplers, Higher Order Mode Couplers and Pick-Up Couplers

RF couplers serve a single purpose for superconducting cavities and linacs, and that is transporting power. There are three basic types of couplers used for this objective,

fundamental power couplers, higher order mode (HOM) power couplers, and pick-up couplers. These three types of couplers serve very different functions. The role of the FPC is to transport RF power to the cavity, while the pick-up and HOM couplers remove power from the cavity.

Pick-up couplers are also used to extract power from the cavity in order to measure the transmitted power. These are typically very weakly coupled in order to prevent large amounts of power from being removed. Pick-ups use a simple geometry based on commercially available N-type feedthroughs.

FPCs are designed to operate at the resonant frequency of the cavity. This frequency can vary depending on several factors, such as the temperature, pressure, or tuning of the cavity, however this range is rather small. The amount of power that is input to a cavity can be up to several megawatts, transmitted either CW or pulsed. More information on current activities involving pulsed and CW input power couplers can be found in the presentation by Garvey [9]. When there is no beam in the cavity, nearly all of the input power is reflected back through the coupler, as the cavity losses are quite small. This reflected power creates a standing wave with twice the voltage and current. Thus an input coupler must be capable of handling four times the forward power.

Section 2.1 explained how time-varying fields impart energy to the beam. The converse is true as well, the charge moving through the cavity can excite higher order modes. HOMs do not provide useful acceleration and can be detrimental to the beam stability. Additionally, these modes also increase the cryogenic load due to the added power dissipated in the walls of the cavity. The higher the beam current is, the more excitation of HOMs occur. A method of determining these modes is given in the thesis by Popielarski [20]. HOM couplers are used to extract power from the cavity only at frequencies higher than the fundamental. The design of the HOM coupler must ensure that it does not couple to the accelerating mode, as this will produce a

degradation in the cavity performance and additional RF power dissipation for the HOM load. There are two types of HOM couplers [14]. The first carry the power away from the cavity to be dissipated in an external load. The second type of coupler uses RF absorbers embedded in the coupler walls to dissipate the energy within the module. The QWRs being used have only three modes total, and are designed for low beam current, so extracting the HOM power is not necessary. The focus of this thesis is the design and analysis of a FPC, but the processes and methods are similar for designing HOM couplers as well.

3.2 Coupling Methods and Locations

Many coupler geometries are possible, but the two most common are the waveguide and coaxial. Both methods of coupling have benefits and drawbacks. There is not a clear advantage that makes one style the best for all applications. Table 3.1 provides a quick comparison of these two types of couplers [21].

Table 3.1: Comparison of coaxial and waveguide couplers.

	Pros	Cons
Waveguide	•Simple design •High power •Simple cooling •High pumping speed	•Large •Large heat load •Difficult variability
Coaxial	•Compact •Small heat leak •Coupling variability •Adjustable impedance	•Complicated design •Lower power •Complicated cooling •Slow pumping speed

Waveguide couplers are less complicated, and many styles and frequencies are readily available from industry. Waveguide couplers are capable of handling large amounts of power. The simple geometry of a rectangular waveguide makes it easy to cool and the open structure allows high vacuum pumping speed. One major drawback

of the waveguide coupler is its size, especially at low frequencies. The dominant mode of a rectangular waveguide is the TE_{01} mode [22]. The cutoff wavelength of a waveguide is

$$\lambda_c = 2d \tag{3.1}$$

where d is the width of the waveguide. Thus the width of the waveguide must be larger than one-half of the wavelength corresponding to the desired operating frequency of the cavity. A 80.5 MHz waveguide would be 1.86 meters wide, but only 50 millimeters wide at 3 GHz. Therefore waveguides are not typically used for frequencies less than 500 MHz.

Although waveguide couplers provide several mechanical benefits, coaxial couplers have one distinct advantage. That advantage is the ability to change the impedance of the coupler to provide different matching conditions. A coaxial coupler can also be more compact. Additionally, the coaxial coupler is basically a transmission line, so multiple frequencies are able to propagate. This allows a single design to be used for different frequencies if necessary. The condensed geometry of this type of coupler generally allows for a smaller heat load, at the expense of slower vacuum pumping speed. Another asset of the coaxial design is the ability to make the coupling adjustable. It is possible to make an adjustable waveguide coupler, however, it is much more complicated.

Just like there are two common types of input couplers, there are also two methods of coaxial coupling to a cavity. The first is coupling to the magnetic field using a current loop, and the second is using a voltage probe to couple to the electric field. Using Equation (2.13) and Figure 3.1, we can see that the peak magnetic field is near the top of the cavity and is azimuthal. Therefore a loop antenna would be ideally placed near the top of the cavity, where the magnetic field is the strongest. The coupling strength can then be adjusted by changing the size and orientation of the loop. Figure 3.2 and Equation (2.14) show the peak electric fields are located at the

tip of the inner conductor, near the bottom of the cavity. The electric field is radial, and decreases along the length of the cavity. Ideally, the probe would be located along the beam axis where the electric fields are strongest, but the bottom of the cavity is close to the peak fields and allows for a simpler mechanical design. The coupling strength can be adjusted by the voltage probe's length and diameter.

Most accelerators use fixed coupling, since the beam current is fixed and loading is well defined [13]. If there is a large amount of beam loading, and the range of the beam current is too great to be compensated by the RF controls alone, a variable coupler can be used. This variability requires more complex feedthroughs and actuators for control. In the case of voltage probe type couplers, a linear actuator can be used to increase the amount of penetration. Current loops can use a linear or rotary actuator to change the magnetic flux through the loop. The easiest method to move either of these would be to put the actuator inside the cryomodule, and run the controls out of the module. However, it is difficult to find reliable actuators that operate at cryogenic temperatures. Externally mounted methods are more reliable, but require actuator feedthroughs that can transmit motion and still maintain vacuum. Additionally, it is sometimes difficult to achieve strong coupling without disturbing the cavity fields.

3.3 RF Window

The main function of the RF window is to isolate the cavity vacuum from the atmosphere while transmitting RF power through the coupler. There are several aspects that require consideration when designing a window. One of the first issues that needs to be addressed is the window location. If the window is located inside the module it is considered a cold window. This method allows the cavity to be completely sealed while still inside the clean room. However this approach is more complicated as it requires vacuum on both sides of the window. Additionally, because this window is close to the cavity itself, and is more prone to damage from electrons and x-rays

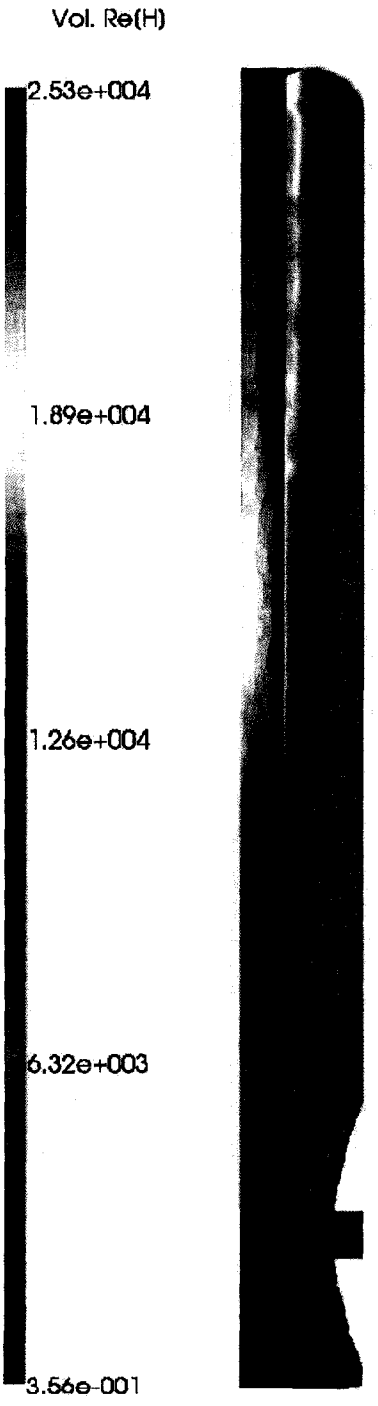

Figure 3.1: Analyst model of $\beta = 0.041$ QWR showing the surface magnetic field distribution.

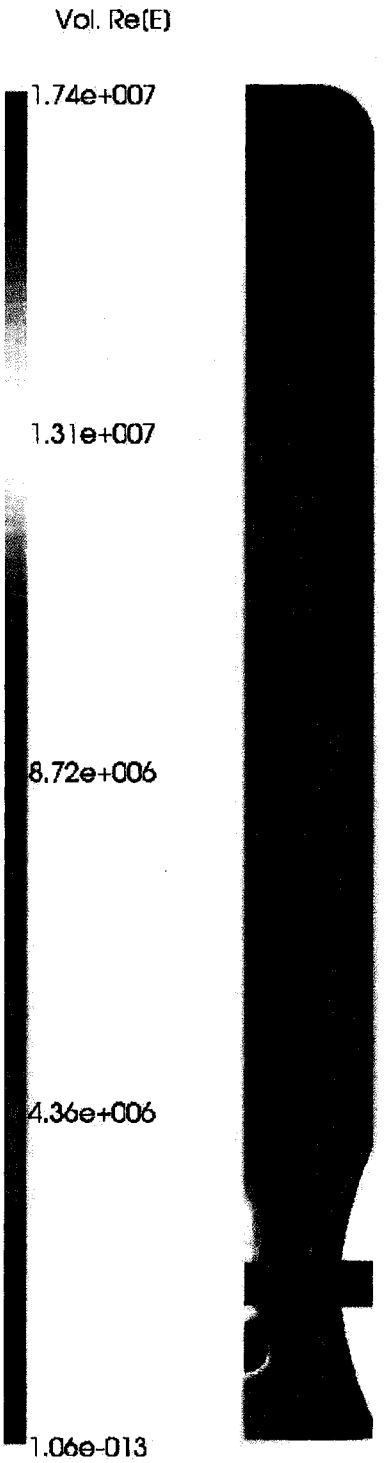

Figure 3.2: Analyst model of $\beta = 0.041$ QWR showing the surface electric field distribution.

emitted from the cavity [15]. The electrons can charge up the window and create arcing. As clean room procedures have improved, sealing the cavity early on is not as important as it once was. The warm window has become more popular, as it does not have the drawbacks of the cold window. This method is preferred for high power applications because any multipacting or RF heating that occurs at the window is far away from the cavity. Some facilities opt to implement double windows to provide extra protection. The warm window design used in our application has the benefit of sealing the cavity while it is still inside the clean room. The cryomodule construction is such that each of the completed coupler assemblies can be inserted through the cryomodule walls.

Another important design consideration is the geometry of the window. This is often decided by the type of coupler used. Waveguide couplers typically rely on planar windows mounted in the waveguide. These windows can be rectangular, or can consist of one or more circular disks brazed to a vacuum tight flange. In the case of coaxial couplers, the window requires a hole in the center for the inner conductor to pass through. This window is usually a cylinder, disk, or cone. Conical windows can be used for impedance matching, but it is not clear if it provides any benefit against multipacting.

3.4 Material Considerations

Common materials used in power couplers include stainless steel, oxygen-free high-conductivity (OFHC) copper, and ceramics. The ceramic that is most common is high purity alumina (> 95% AL203)[1]. Although it has low thermal conductivity (30 W/mK), it is often chosen because of its availability and purity. The thermal conductivity of alumina does increase as the temperature decreases, making it advantageous

[1] ISI refers to (> 95%) as high purity, but other sources consider it medium purity, and (> 99%) as high purity [13]

for cold windows. Knife-edge flanges are commonly made from stainless steel, and are sealed together with copper gaskets. Selecting the materials for the rest of the coupler is slightly more complex.

One issue that the coupler materials present to the cryogenic system is a thermal load. It takes approximately 1 kW of electric power to remove 1 W of heat from liquid at 2 K due to Carnot losses and inefficiencies. Therefore it is important to minimize both the RF heating and the thermal leakage to the cold mass at 2 to 4.5 K. The thermal conductivity of stainless steel is much lower than that of copper, as shown in Figure 3.3 [23]. AISI 317 stainless steel appears to be the best choice of material for the outer conductor to minimize heat transfer. However, another source of heating is from the ohmic losses inside the outer conductor. The electrical resistivity of stainless steel is much greater than that of copper, as presented in Figure 3.4. OFHC copper would be the preferred outer conductor material to minimize the ohmic losses, but it would transfer too much ambient heat into the module. A compromise must be made between thermal conduction and ohmic losses. The solution is to plate the interior surface of the stainless steel outer conductor with a layer of copper. The majority of the conductor is stainless steel with poor thermal conductivity, while the copper lining is sufficient to reduce the ohmic losses. The thermal conduction along the copper inner conductor is not an issue because it is not in direct contact with the helium system, so there is no path for the heat to conduct.

3.4.1 Calculating Heat Load and RF Losses

The total static heat leak from the RF input coupler can be estimated from the sum of the calculations for both the inner and outer conductor. The total heat leak includes the case when the RF is turned on and includes the RF power conducted along the coupler [24]:

$$q_{total} = q_{cond} + q_{rad} + q_{rf} \tag{3.2}$$

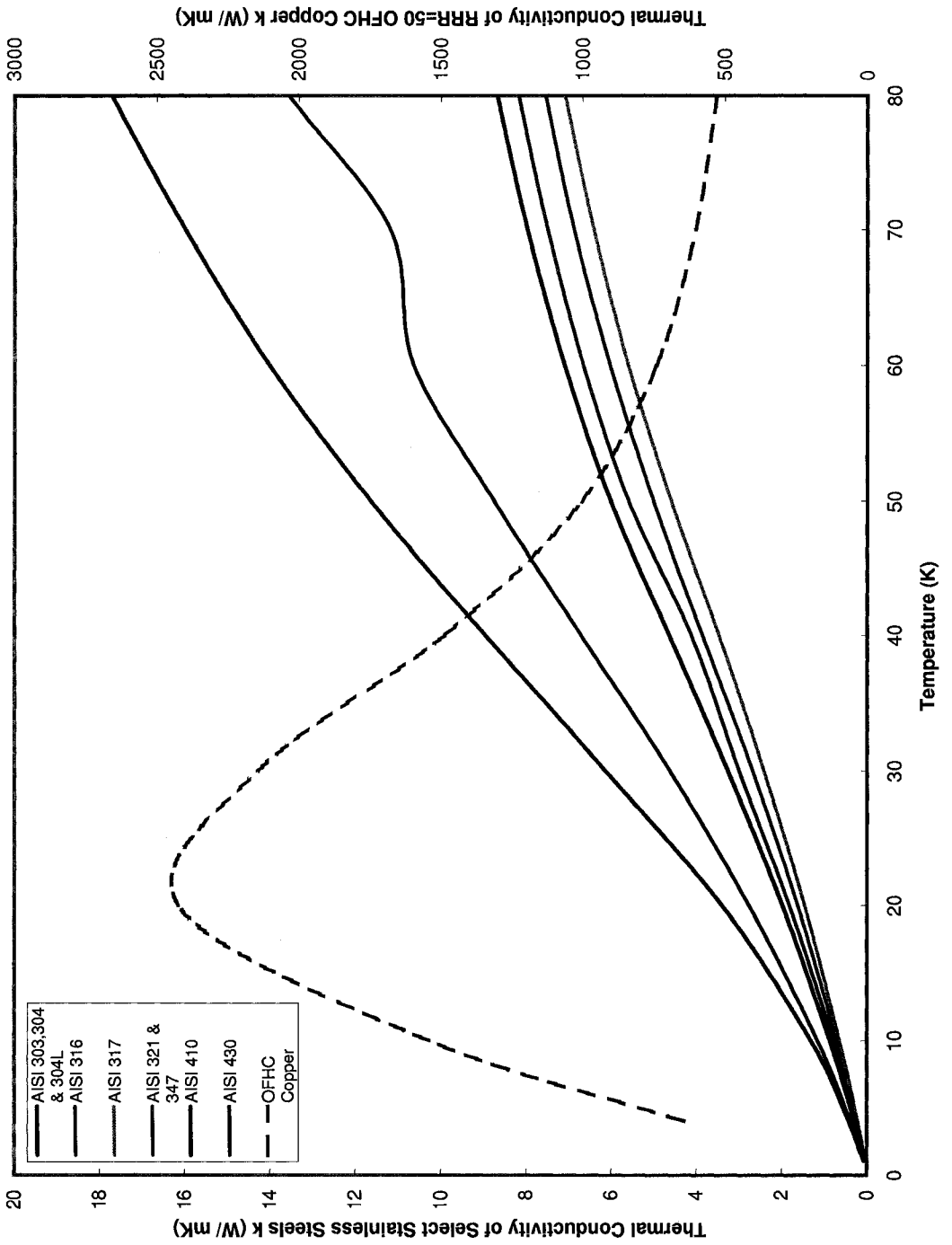

Figure 3.3: Thermal conductivity of OFHC copper and select stainless steels.

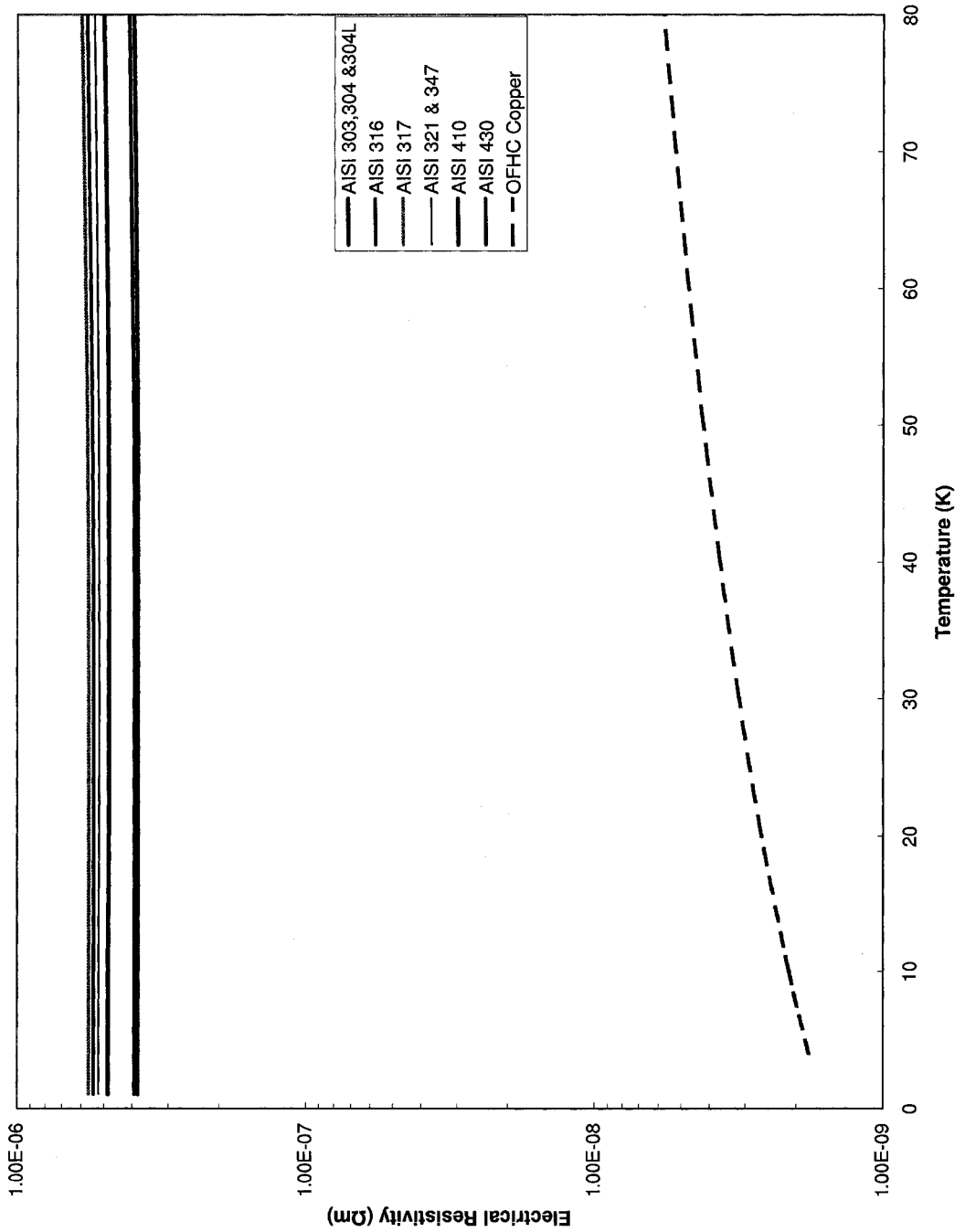

Figure 3.4: Electrical resistivity of OFHC copper and select stainless steels.

where q is the heat transfer in watts. The RF conduction heat leak is estimated from [25]

$$q_{rf} = \frac{1}{2} I^2 \frac{\rho x}{2\pi r \delta} \tag{3.3}$$

where I is the current, ρ is the temperature dependent resistivity, x is the length of the coupler, r is the radius of the outer conductor, and δ it the skin depth. The skin depth can be expressed as

$$\delta = \sqrt{\frac{1}{\pi f \mu_o \sigma}} \tag{3.4}$$

where σ is the conductivity of the material

$$\sigma = \frac{1}{\rho} \tag{3.5}$$

The static heat leak radiated from the center conductor (and absorbed by the outer conductor, thus contributing to the total heat leak) is calculated from the temperature dependent equation [26]:

$$q_{rad} = \frac{\sigma_{SB} A_{ic} (T_{ic}^4 - T_{oc}^4)}{\left(\frac{1}{\epsilon_{ic}}\right) + \left(\frac{A_{ic}}{A_{oc}}\right)\left[\frac{1}{\epsilon_{oc}} - 1\right]} \tag{3.6}$$

The inner conductor is assumed to be a constant temperature (400 K) and the emissivity (ϵ) is 0.3 and the Stefan-Boltzmann constant (σ_{SB}) is 5.6703×10^{-8} W/(m^{2}K^4)

The heat conduction in the outer conductor is calculated from the sum of the temperature dependent thermal conductivities of copper and stainless steel, wall thickness and plating thickness:

$$k(T)A = k_{ss}(T)A_{ss} + k_{cu}(T)A_{cu} \tag{3.7}$$

This equation is solved from the desired heat leak, $q_{cond} = Ak(T_2 - T_1)/dx$, and a temperature profile can then be calculated from a given geometry. The minimum

distance to the 77 K intercept can then be found for a given q_{cond}.

The heat transfer model includes the calculation of the heat conducted to the 4.5 K helium bath from the 77 K intercept, the radiated heat from the center conductor, and the ohmic losses due to the RF standing wave, using the losses in each skin depth.

3.5 Conductor Sizing

The first concern of determining the conductor geometry is matching the impedance of the coupler to the power amplifier. Since η_o is the impedance of free-space and can be found by

$$\eta_o = \sqrt{\frac{\mu_o}{\varepsilon_o}} \approx 120\pi\ \Omega \tag{3.8}$$

the desired diameter of the outer conductor for a coaxial line can be calculated from [27]

$$Z_o = \frac{\eta_0 \ln(b/a)}{2\pi} \approx 60 \ln\left(\frac{b}{a}\right) \tag{3.9}$$

where a and b are the diameters of the inner and outer conductors, respectively. The reflection coefficient of the coupler can be calculated using [28]

$$\Gamma_L = \frac{R_L - Z_o}{R_L + Z_o} \tag{3.10}$$

The reflected power is then calculated by

$$P_r = |\Gamma_L|^2 P_f \tag{3.11}$$

The more dramatic coupler mismatch occurs at the window transition where the dielectric changes from air to alumina. To calculate the impedance of a partially filled

coaxial line, the following formula can be used [29]

$$Z_g = \frac{Z_o}{\sqrt{\frac{\theta}{360}\left[\frac{\varepsilon_2 \ln(b/a)}{\varepsilon_1 \ln(c/a)+\varepsilon_2 \ln(b/c)} - 1\right] + 1}} \tag{3.12}$$

Figure 3.5 shows the geometry for Equation (3.12), a is the inner conductor diameter, b is the outer conductor diameter, c is the diameter of the second dielectric, θ is the angle the second dielectric occupies, ε_2 is the relative permittivity of alumina, and ε_1 is the relative permittivity of free space. The relative permittivity of alumina ranges from 7.1 to 10.5 depending on the purity [30].

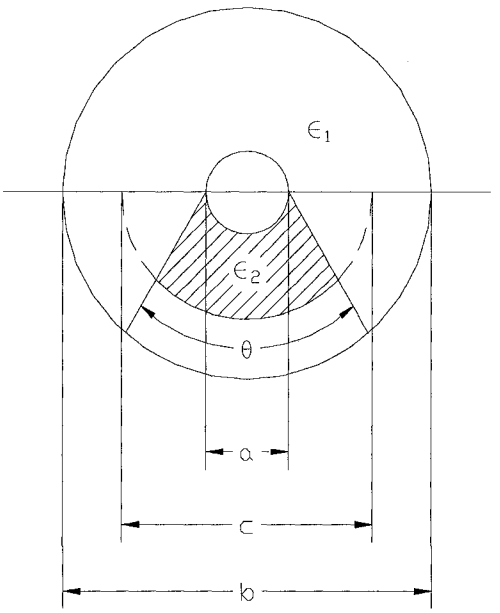

Figure 3.5: Geometry of partially filled transmission line.

Another issue that depends on the size of the conductors is multipacting. Multipacting occurs when an electron is emitted from the surface of a conductor, gets accelerated by the electric field and then impacts the surface, creating secondary electron emissions. These new electrons then repeat the process, resulting in large power losses and conductor heating. This electron activity can limit the performance

of a coupler. Multipacting trajectories are not always fully understood, and complex geometries make it difficult to predict multipacting behavior. Mathematical codes have been developed to analyze simple coaxial geometries and have shown that multipacting in the lines are due only to the electric field [31]. The multipacting levels were found to scale with frequency, conductor size, and line impedance according to

$$P_{one-point} \sim f^4 b^4 Z^1 \tag{3.13}$$

for one-point multipacting and

$$P_{two-point} \sim f^4 b^4 Z^2 \tag{3.14}$$

for two-point multipacting, where b is the diameter of the outer conductor.

Other measures besides changing coupler size or frequency can be taken to reduce multipacting in alumina windows. One method is to apply titanium-based coatings to the ceramic via sputtering [14]. The most commonly used coating is titanium nitride (TiN). The slight conductivity of these coatings allows charge drainage, preventing electrical breakdown [15]. This method adds complexity to the window design and provides mixed results. Another method is media blasting the vacuum side of the window with alumina grit. A detailed analysis of this method and other RF window issues are presented in the dissertation by Cummings [32].

3.6 Finding the External Quality Factor

The external quality factor was introduced in Section 2.1 as the measure of energy lost to the couplers. In cases of heavy beam loading, the Q_{ext} is determined by the beam power. For low beam loading, the Q_{ext} is a determining factor of the system bandwidth. The bandwidth requirements are set by the RF control system, so Q_{ext}

must be properly set to provide the necessary bandwidth. The desired Q_{ext} can be determined using

$$BW = \frac{f_o}{Q_{ext}} \tag{3.15}$$

For a coaxial probe coupler, a simple approach to setting Q_{ext} is to measure it experimentally while varying the coupler inner conductor penetration length.

Q_{ext} can be calculated from three parameters that are easily measured using a VNA. These parameters are the reflection coefficient (S_{11}), the transmission coefficient (S_{21}), and the loaded quality factor (Q_L). The scattering parameters (S-parameters) are frequency dependent and are used to quantify the response of a transmission line with a discontinuity, or network inserted. For a two-port network, the input side is port-1 and the output is port-2. The reflection coefficient is the amount of power reflected from the network back through port-1. The transmission coefficient is the power that is transmitted from port-1 to port-2, through the network.

Padamsee [15] derives the following equations useful in determining the external quality factor. The coupling factor of the input coupler can then be calculated using

$$\beta_{ext,t} = \frac{1 \pm |S_{11}|}{1 \mp |S_{11}|} \tag{3.16}$$

where the upper sign is used if the input antenna is overcoupled, and the lower sign when undercoupled. The coupling factor is never negative. In order to find the coupling factor of the pick-up probe, the transmitted and reflected power need to be accounted for using

$$\beta_{ext,p} = \frac{|S_{21}|^2}{1 - |S_{21}|^2 - |S_{11}|^2} \tag{3.17}$$

Now Equation (2.9) can be used to find the intrinsic quality factor. This Q_o can then be used to find the external quality factor of the pick-up ($Q_{ext,p}$) and input ($Q_{ext,t}$) by applying

$$Q_{ext,p} = \frac{Q_o}{\beta_{ext,p}} \tag{3.18}$$

and

$$Q_{ext,t} = \frac{Q_o}{\beta_{ext,t}} \tag{3.19}$$

respectively. The position of the inner conductor tip has the strongest effect on the coupling between the FPC and cavity [33].

3.7 Potential Faults and Failures

As important as the task of transporting power to the cavity is, coupler windows serve a second, equally significant purpose. This secondary function is protecting the cavity vacuum. The potential for failure seems large with high RF power traveling through a fragile ceramic window. If a failure were to occur, the best case scenario would be a power transmission issue causing the cavity to underperform. The worst case is a vacuum breach that will spoil an entire cryomodule, or multiple cryomodules, requiring disassembly and cleaning of the cavities. It is estimated that the cost of repairing a single failed module due to a broken window is hundreds of thousands of dollars in time and materials [14]. Methods can be been implemented to reduce the probability of a catastrophic failure. Diagnostics and interlocks are used to monitor and prevent the two basic types of coupler faults, barrier and transmission. In fact, most of the interlocks typically used in superconducting cavities are not for the cavities themselves, but rather to protect the couplers [13]. The following addresses several common modes of failure.

Transmission type faults occur when the cavity does not get the RF power necessary to operate properly. These are not as dramatic as barrier faults because the vacuum remains intact. Typically this only affects a single cavity, so if the proper steps are taken, the module need not be removed from the beam line for repair. In fact, if precautions are taken, the coupler can be replaced while the module remains in place. Proper design and engineering of the coupler will minimize transmission

issues. The most common issue is multipacting, which has already been discussed in Section 3.5. Even though the correct coupler geometry is used to minimize multipacting, proper conditioning of the coupler is still necessary to work through these multipacting areas beforehand. Another issue caused by multipacting is the heating of the conductors. This places an undesirable load on the cryogenics system, and reduces coupler performance.

The second, and more critical type of fault is a barrier fault. A barrier fault is any breach in the vacuum of a cavity or module. Causes of this type of fault include any sort of fracture in the window. These can be caused by mechanical shock or an electrical event. It is obvious that forces applied to the coupler window can crack the ceramic material, so caution must be taken during the module assembly and transport. Because of the fragility of the ceramic, and the high cost of failure, coupler diagnostics are usually installed near the alumina window. The devices that are typically used to monitor the window's status are electron probes, spark detectors, and vacuum gauges [15]. The electron probe is used to detect multipacting. If multipacting occurs, current will be observed on the probe, and the forward power can be reduced to protect the window. In addition, multipacting causes a change in pressure due to the electron impacts. This may be observed by the vacuum monitor. Sparks can damage the ceramic, and sputter metal onto it. This reduces the insulating ability of the alumina. Another device that is becoming more common is an infrared (IR) temperature sensor or photo-multiplier [9]. These are used to monitor the temperature of the ceramic for heating due to electron impacts.

Another possible mode of barrier failure is damage to the coupler bellows. The bellows seal the outer conductor to the module and allow movement of the FPC as the components inside thermally contract. These bellows are welded to the outside of the outer conductor and care must be taken while welding. Reliability issues have been observed due to resistance and TIG welding of the bellows to their mating flanges

[34].

These are some of the basic considerations that need to be made when designing a power coupler. Many design issues need to be resolved before prototyping can begin. The next chapter will show how these methods were applied in the development of the fundamental power coupler for ReA3.

Chapter 4

Design Approach and Methodology

The mechanical and electrical design of the coupler occur simultaneously. Choices made in one area will affect the coupler in others. The previous chapter presented some of the considerations for the design of a FPC. This chapter will show how those methods were applied to design the FPC presented in this thesis.

Section 4.1 covers the procedure for determining the coupler placement on both the cavity and cryomodule. The calculations used to minimize the heat losses are in Section 4.2. Once the heat load is found, there is enough information to determine the other conductor sizes, as shown in Section 4.3. Simulation for the coupler window and inner conductor are provided in Section 4.4. After the basic coupler design has been prototyped, the proper length of the inner conductor can be determined experimentally, as is described in Section 4.5. Lastly, Section 4.6 describes the methods used to minimize any coupler operation issues.

4.1 FPC Placement

Using a waveguide coupler is not practical, as the minimum width of a rectangular waveguide is $\lambda/2$, as shown by Equation (3.1). This dimension is approximately twice the length of the quarter-wave cavities that will be used for ReA3. Therefore a

waveguide power coupler is not practical in this application, since the coupler would be bigger than the cavity.

The QWRs that will be used for ReA3 are based on the 80 MHz resonators currently being used at Legnaro for the ALPI and PIAVE linacs [35]. In order to simplify the cryomodule design, electrically coupling through the bottom plate was the method chosen for the FPC presented here.

Coaxial couplers have a smaller geometry, making them the ideal choice for our application. This small footprint allows the input and pick-up coupling ports to be mounted alongside the tuning actuator, as shown in Figure A.3.

Another design consideration is the variability of the coupler. It is anticipated that the beam current for secondary beams will be small, so the coupling can be set by the desired bandwidth, and not by the beam current. Additionally, transmitting motion into the cavity vacuum increases the complexity of the design. Fixed coupling simplifies the coupler design, which makes the design more economical and allows for fewer failure modes.

4.2 Minimizing Heat Load and Losses

Figure 3.3 shows that AISI 317 has the lowest thermal conductivity of the stainless steels listed, and is much lower than that of OFHC copper. This makes it the best material for the outer conductor. However AISI 316 stainless steel was chosen because its thermal conductivity is very close to that of AISI 317, and it is readily available in many standard tubing sizes.

In section 3.4, we showed that copper plating the interior surface of the stainless steel outer conductor reduces the ohmic losses in the material. It is necessary to calculate the plating thickness which minimizes the ohmic losses without increasing the thermal load. Additionally, the minimum outer conductor length must be found: If the conductor is too short, additional heat leaks into the module. The analysis of

Section 3.4.1 was performed for various plating and wall thicknesses and the results are provided in Table 4.1. The calculations were done using the skin depth of OFHC copper at 77 K of 4.1×10^{-6} meters, which was determined using Equation (3.4). 77 K is the temperature of the nitrogen intercept, and was chosen as a compromise between the cavity end of the outer conductor at 4.5 K and the opposite end at 300 K. Also note that Q_{STAT} does not include the RF losses, so $Q_{TOT} = Q_{STAT} + Q_{RF}$.

The results suggest that $4 - 8$ μm of copper plating should be applied to the minimum practical stainless steel wall thickness. Extending the distance to the 77 K intercept could compensate for thicker stainless steel walls, though slightly increasing both the static and dynamic loads. Thicker copper plating would increase the static load, and an incorrect plating procedure could increase the total load. The analysis also showed that 0.020″ stainless steel wall thickness with no copper plating provided a very low static load (< 0.5 W) and a 1.5 W total heat load due to the RF losses in the stainless steel. The unplated conductor was tested as well as the plated, and the results of that test are discussed in Section 5.5.

Table 4.1: Power coupler heat load analysis.

Q_{STAT} (W)	Q_{TOT} (W)	t_{ss} (")	t_{cu} (skin depths)	L_{min} (")
0.9	1.6	0.020	$1 - 2$	5.0
1.0	1.8	0.035	$1 - 2$	8.0
1.1	2.0	0.060	$1 - 2$	11.0

4.3 Determining Conductor Dimensions

The RF generation system that will be used for ReA3 will have a 50 Ω impedance, so this was the starting point for calculating the coupler impedance. The commercial feedthrough used in this design has an inner conductor diameter of 0.375″. This information allows Equation (3.9) to be used to determine the inside diameter of the

outer conductor. The optimal inside diameter was found to be 0.862″. As mentioned in Section 4.2, standard tubing sizes were used in order to keep the design simple. The AISI 316 outer conductor was made from stainless steel tubing with an outside diameter of 1.0″ and a wall thickness of 0.035″. Thus, the tubing has an inside diameter of 0.930″. Substituting this back into Equation (3.9) results in a coupler impedance of 54.5 Ω.

The process was repeated to determine the impedance of the alumina window. Using Equation (3.12), with $\varepsilon_2 = 9.0$ for high purity alumina, $\theta = 360°$ because the alumina is completely surrounding the inner conductor, and $Z_o = 54.5\ \Omega$, the impedance of the window transition was calculated to be 35.8 Ω.

Calculating the reflection coefficient using Equation (3.10) gives a Γ_L of 0.043 at the coupler transition, and Γ_W of -0.166 at the window transition. Applying Equation (3.10), for 1 kW of forward power, the reflected power was found to be less than 2 W at the coupler, and 27.4 W at the window. The power reflected at the window is acceptable, but can be reduced through optimization. Therefore the stainless steel tubing selected will be suitable for this application.

Multipacting was another geometry issue that was addressed. Using the analysis method described in Section 3.5, it was found that the power levels at which the multipacting would occur are much less than the operating power of either cavity. Because of this, if the coupler can be conditioned and barriers overcome, then multipacting is not expected to be an issue during normal operation.

4.4 Ceramic Window Simulations

With the coupler geometry chosen, the window assembly was simulated in order to find peak field areas and simulate the S-parameters. The first step was to draw a three-dimensional model of the vacuum space surrounding the window. The full

scale model shown in Figure 4.1 was drawn using a 3D CAD program (SolidWorks[1]) mechanical design software. Because the window is axisymmetric, only one-quarter of the window assembly was modeled. This reduced the complexity of the simulation and mesh. The mechanical model was then imported into a finite element electromagnetics solver (Analyst[2]), for field analysis and S-parameter calculations.

Care was taken to model the coupler as closely as possible to the final design. The model was created using five different components, three alumina and two vacuum sections, in order to correctly apply boundary conditions in Analyst. Figure 4.2 shows that the peak electric fields occur on the air side of the window, near the braze joint of the ceramic to the flange. This could be a potential issue: if that area experiences too much heating, the braze joint could fail. The high magnetic field regions are along the inner conductor near the braze joint of the alumina to the inner conductor, as shown in Figure 4.3. The magnetic field is not as large as the electric field, and is not much of a concern.

Although the fields in the final coupler were discussed above, there were several iterations of the coupler design simulated. 'FPC1' was the model of the existing coupler that was being improved upon, and 'FPC2' was the first iteration in the coupler redesign. Although FPC2 appeared to have the best performance, as shown in Figures 4.4 and 4.5, the coupler diameter was too large to properly fit under the QWR. 'FPC3' was the first iteration of the final design. 'FPC4' and 'FPC5' are modifications of the earlier models to accurately reflect the geometry. The design that is presented in this thesis is 'FPC5' and was the best compromise between performance and size. At 80.5 MHz the new window performs better than the existing design, with less reflection and better transmission of power. For operation at higher frequencies, the new coupler will need to be modified in order to improve the performance.

Another simulation that was necessary was the modal analysis of the vacuum

[1] A product of Dassault Systèmes SolidWorks Corp., Concord, Massachusetts.
[2] A product of Simulation Technology and Applied Research, Inc., Mequon, Wisconsin.

Figure 4.1: A 3D model of the coupler window assembly. The blue areas are vacuum space, and the orange ones are high purity alumina.

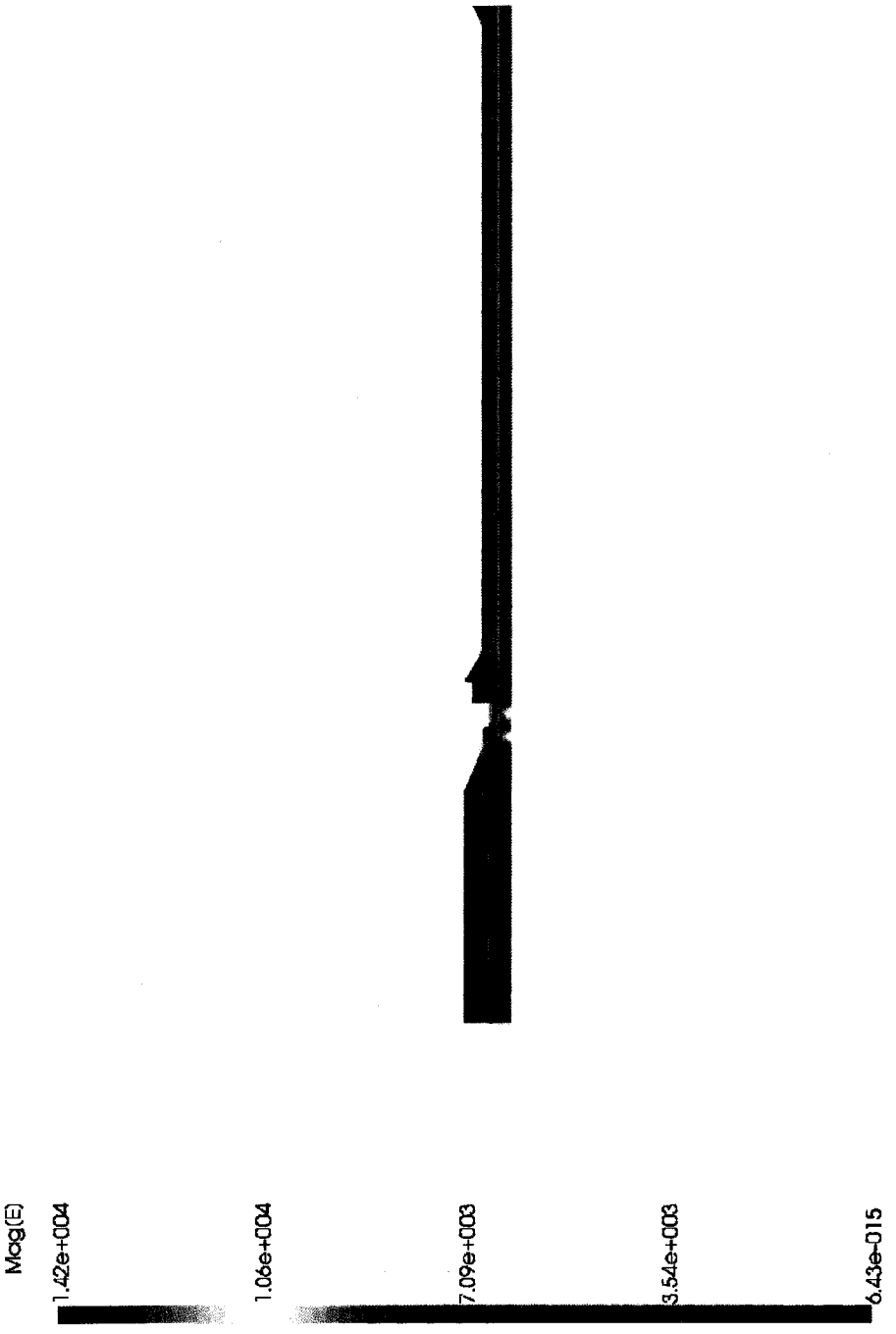

Figure 4.2: Analyst simulation of the electric field in the coupler window assembly.

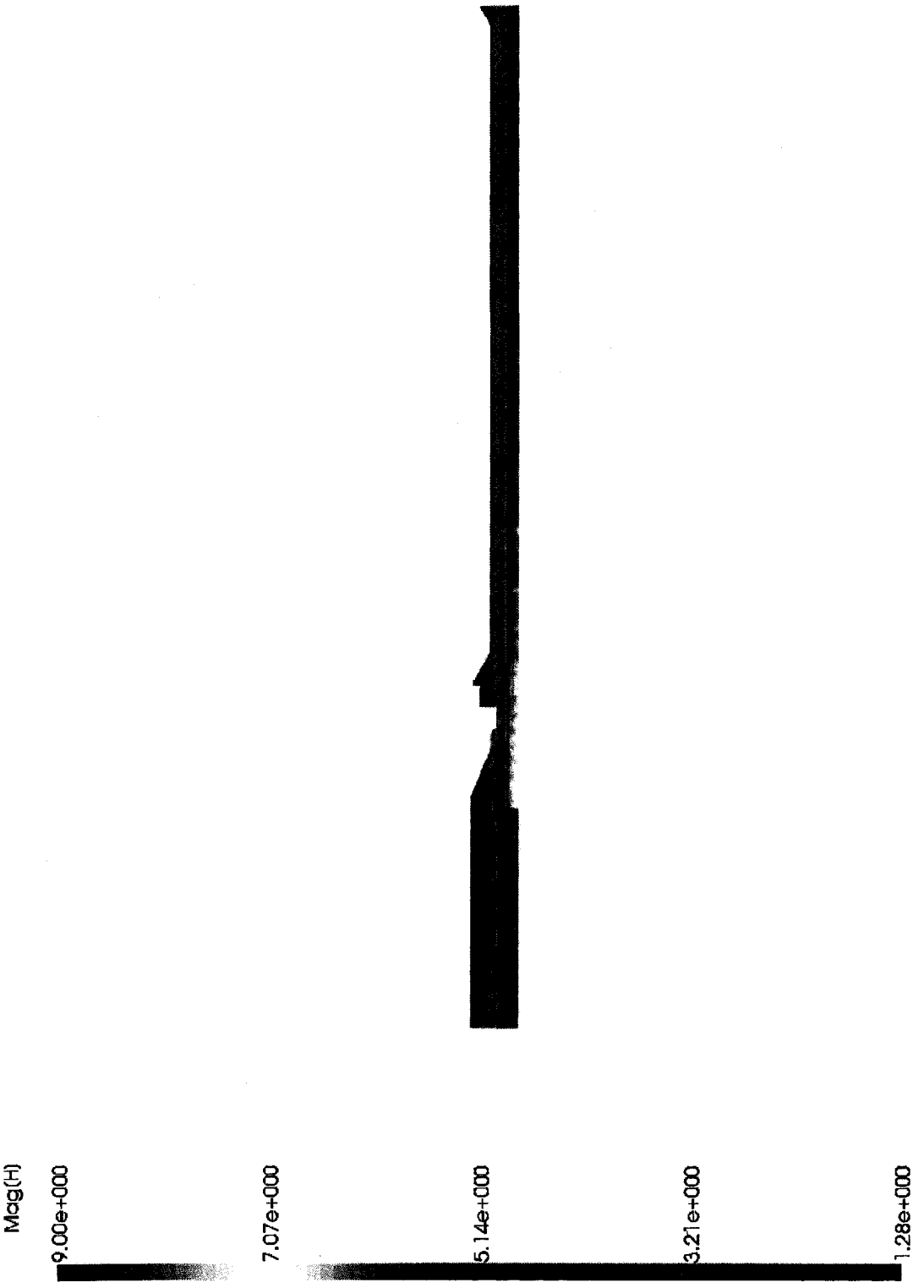

Figure 4.3: Analyst simulation of magnetic field in the coupler window assembly.

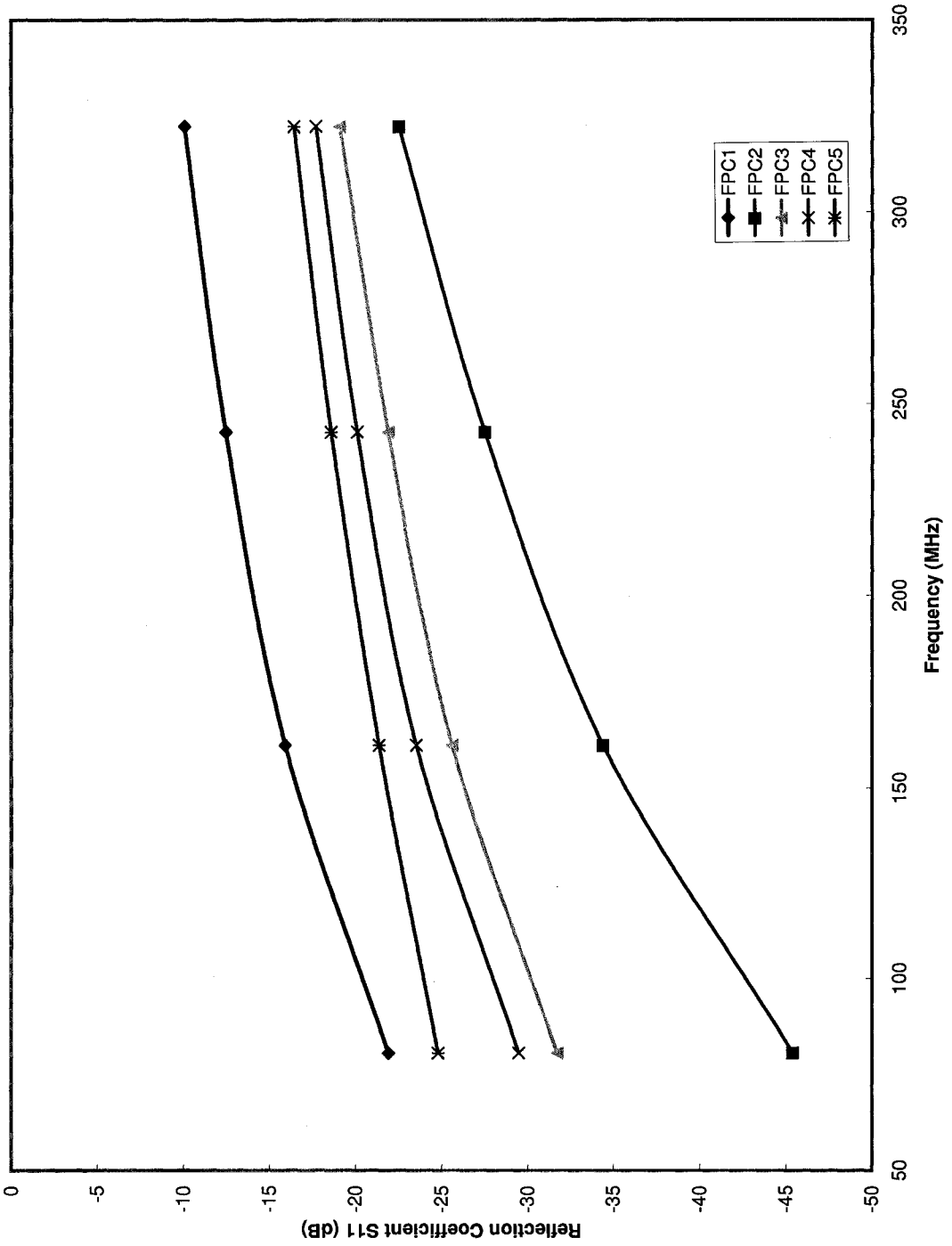

Figure 4.4: Simulated reflection coefficients of selected coupler window assemblies using Analyst.

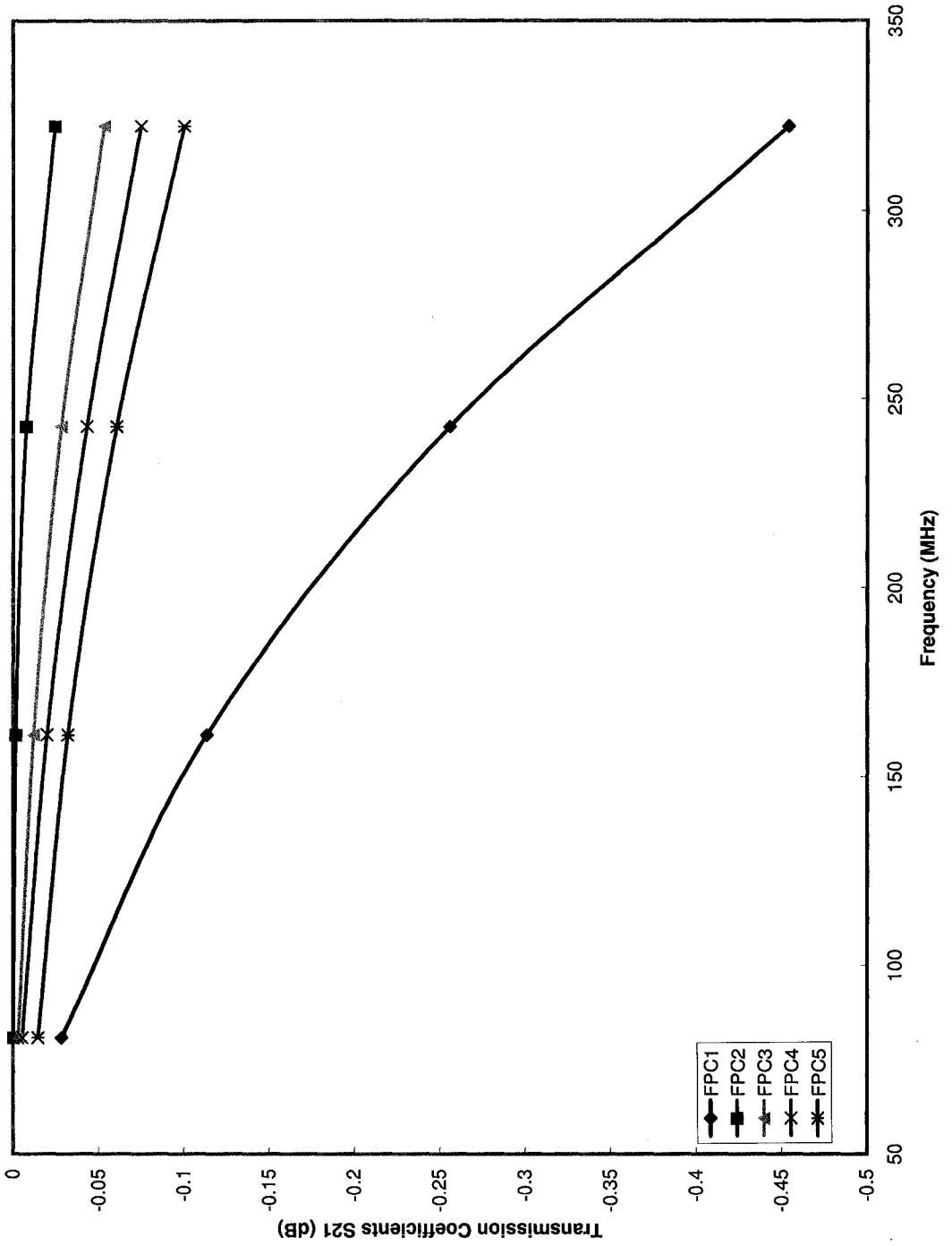

Figure 4.5: Simulated transmission coefficients of selected coupler window assemblies using Analyst.

feedthrough. The inner conductor is only supported by the braze joint at the coupler window, which is over 14" away from the tip. The conductor can be thought of as an inverted pendulum with a stationary base. The analysis of the coupler oscillations was performed using a finite element analysis and computational solver (ANSYS[3]) to find the resonant frequencies of these vibrations. The simulations were performed using the designed inner conductor with various length stainless steel liners inserted. The results are shown in Table 4.2. The mechanical mode of the as-built feedthrough was also measured, and the first harmonic was measured at approximately 28 Hz, very close to the simulated result. The conductor deformation for first three modes, with the 11″ liner are shown in Figures 4.6 through 4.8. The simulations and measurements show that the most desirable method for minimizing tip deflection is using the 11" stainless steel liner, whose displacement is shown in Figure 4.9. By applying the stiffening liners, the amount the conductor will move is reduced, and the resonant frequency of the vibrations is shifted further away from 30 Hz. This is a common frequency of microphonic vibrations in the testing facility.

Table 4.2: Mechanical mode analysis for inner conductor deformation with various length stainless steel liners.

Harmonic	Copper Only	7″ SS Liner	9″ SS Liner	11″ SS Liner
1	28.96 Hz	36.00 Hz	36.63 Hz	36.27 Hz
2	199.45 Hz	201.70 Hz	199.63 Hz	205.02 Hz
3	579.67 Hz	575.40 Hz	581.52 Hz	573.65 Hz

4.5 Setting Q_{ext}

After the geometry was selected, the design changes were submitted to the manufacturer in order to have a semi-custom RF feedthrough engineered. The coupler design ultimately used for this thesis is shown in Figure 4.10 and makes use of a modified RF

[3] A product of ANSYS, Inc., Canonsburg, Pennsylvania.

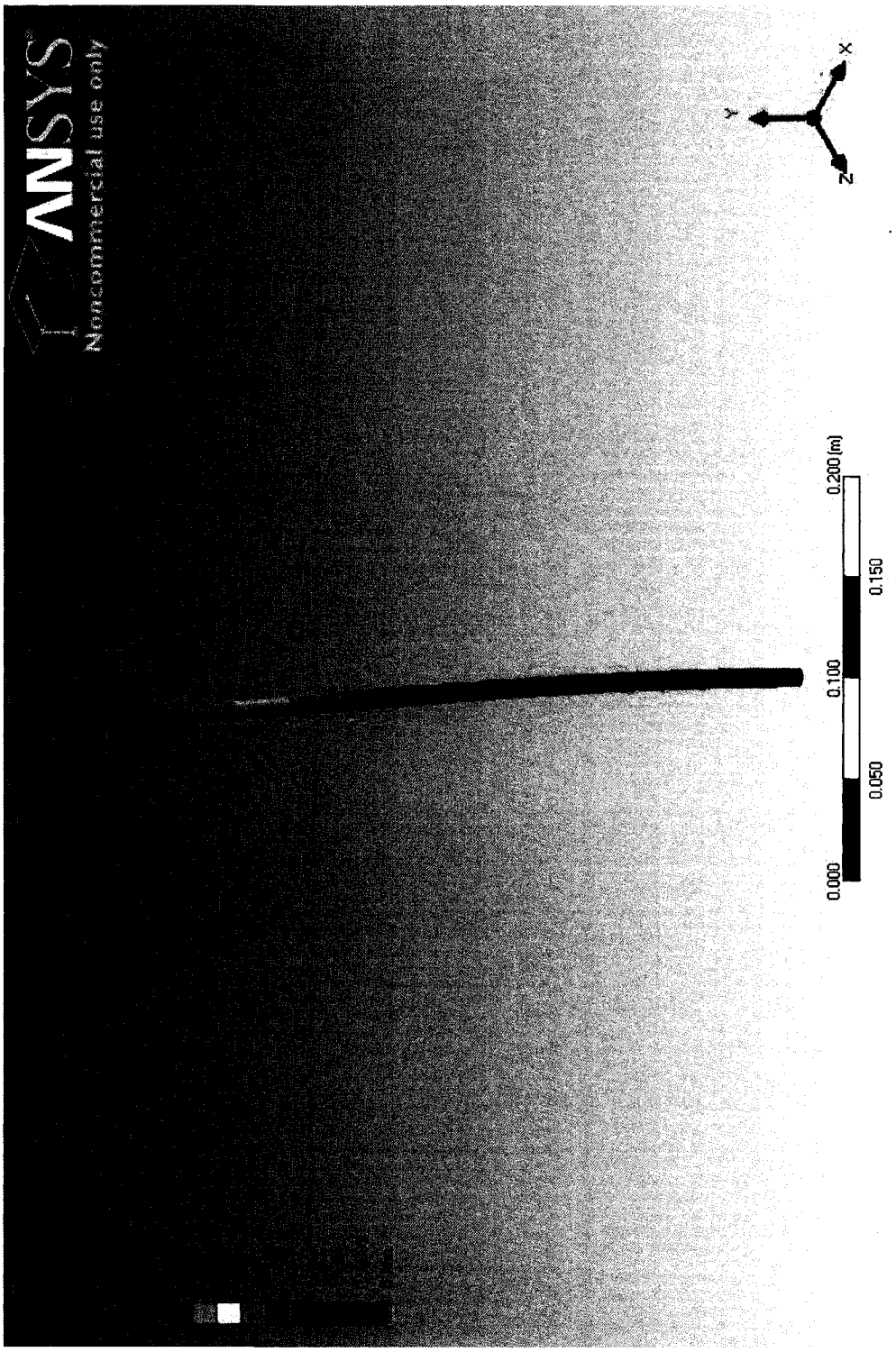

Figure 4.6: ANSYS simulation for the first harmonic deformation of the inner conductor with a 11″ stainless steel liner.

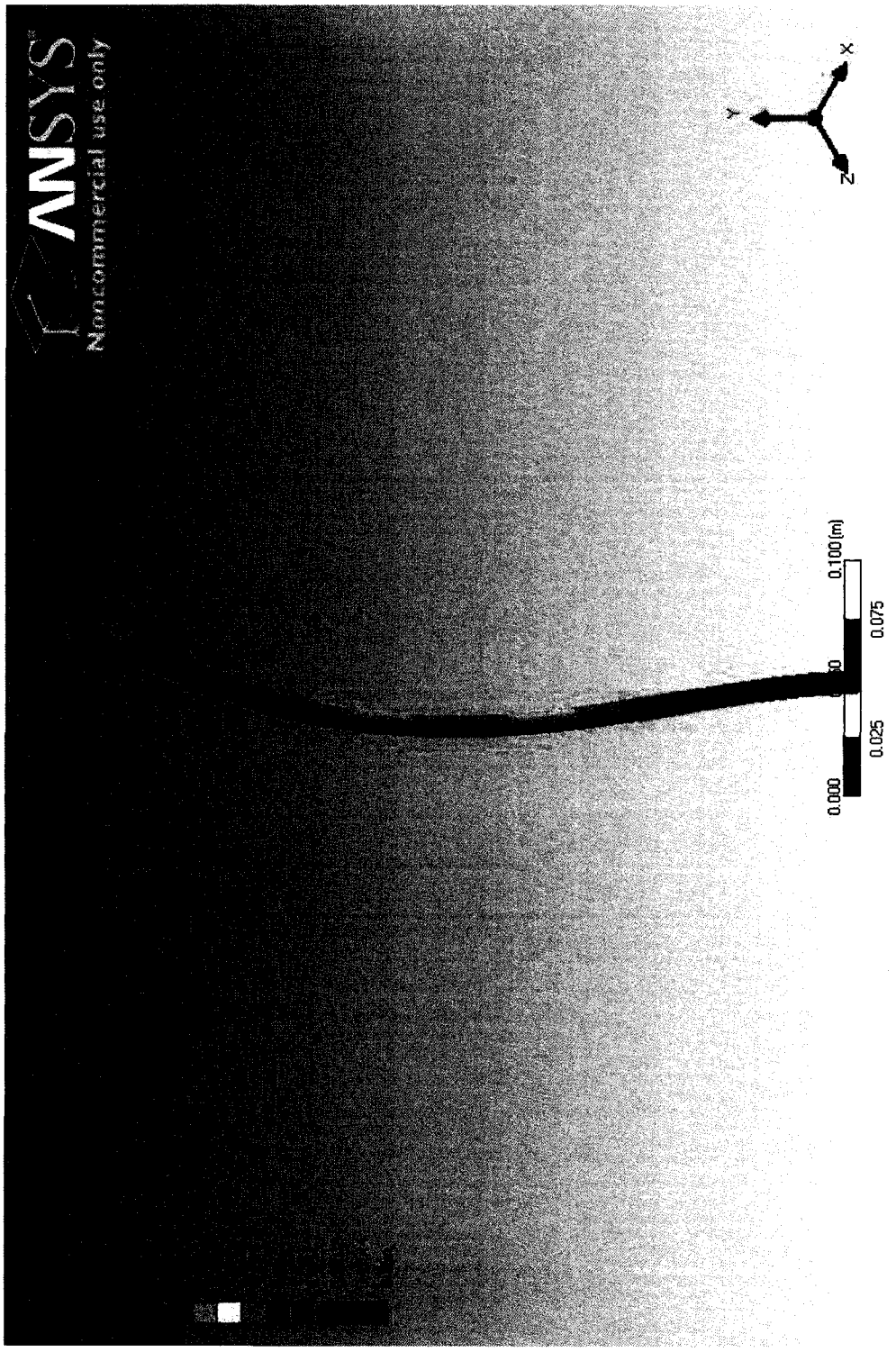

Figure 4.7: ANSYS simulation for the second harmonic deformation of the inner conductor with a 11″ stainless steel liner.

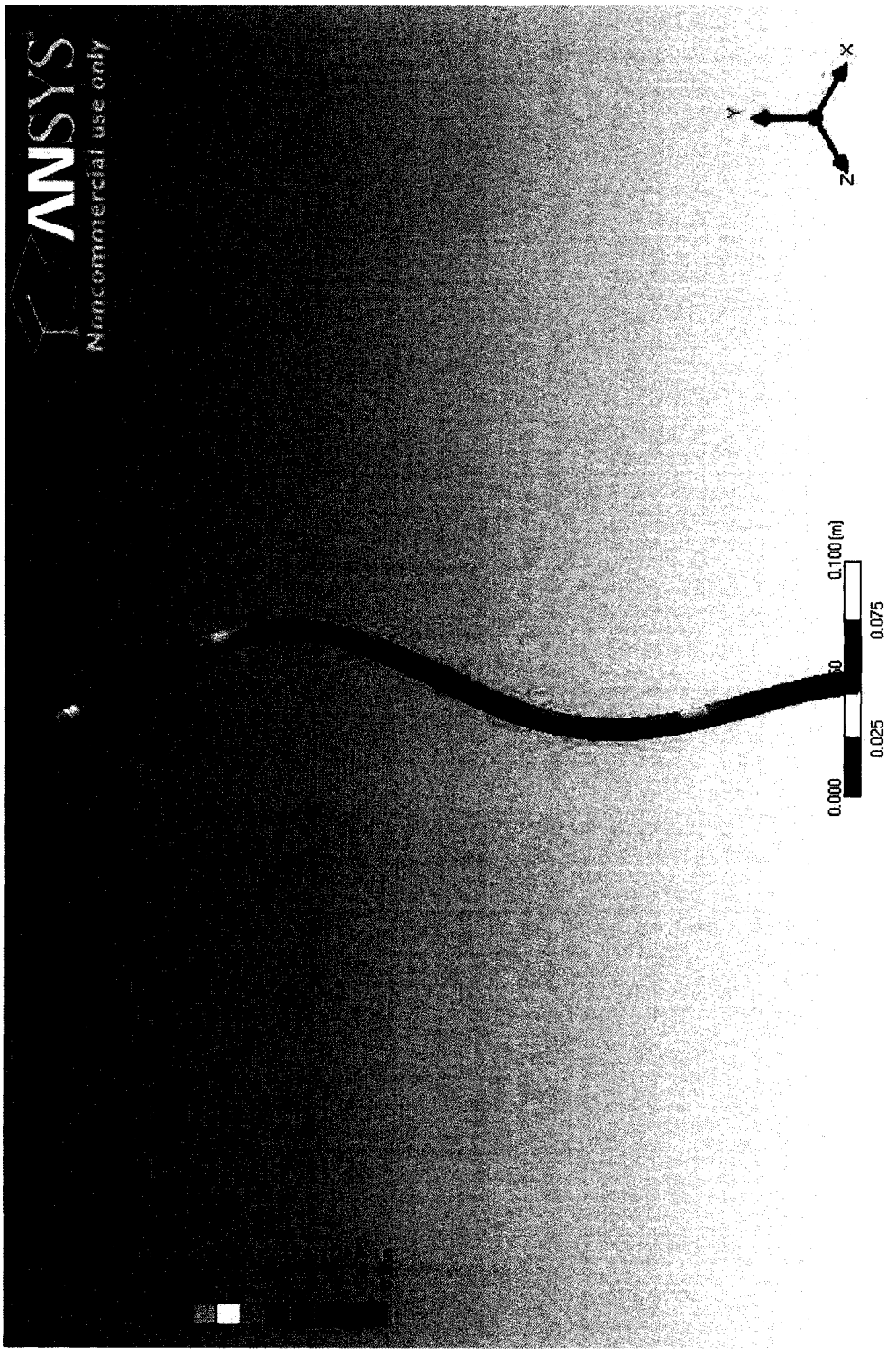

Figure 4.8: ANSYS simulation for the third harmonic deformation of the inner conductor with a 11″ stainless steel liner.

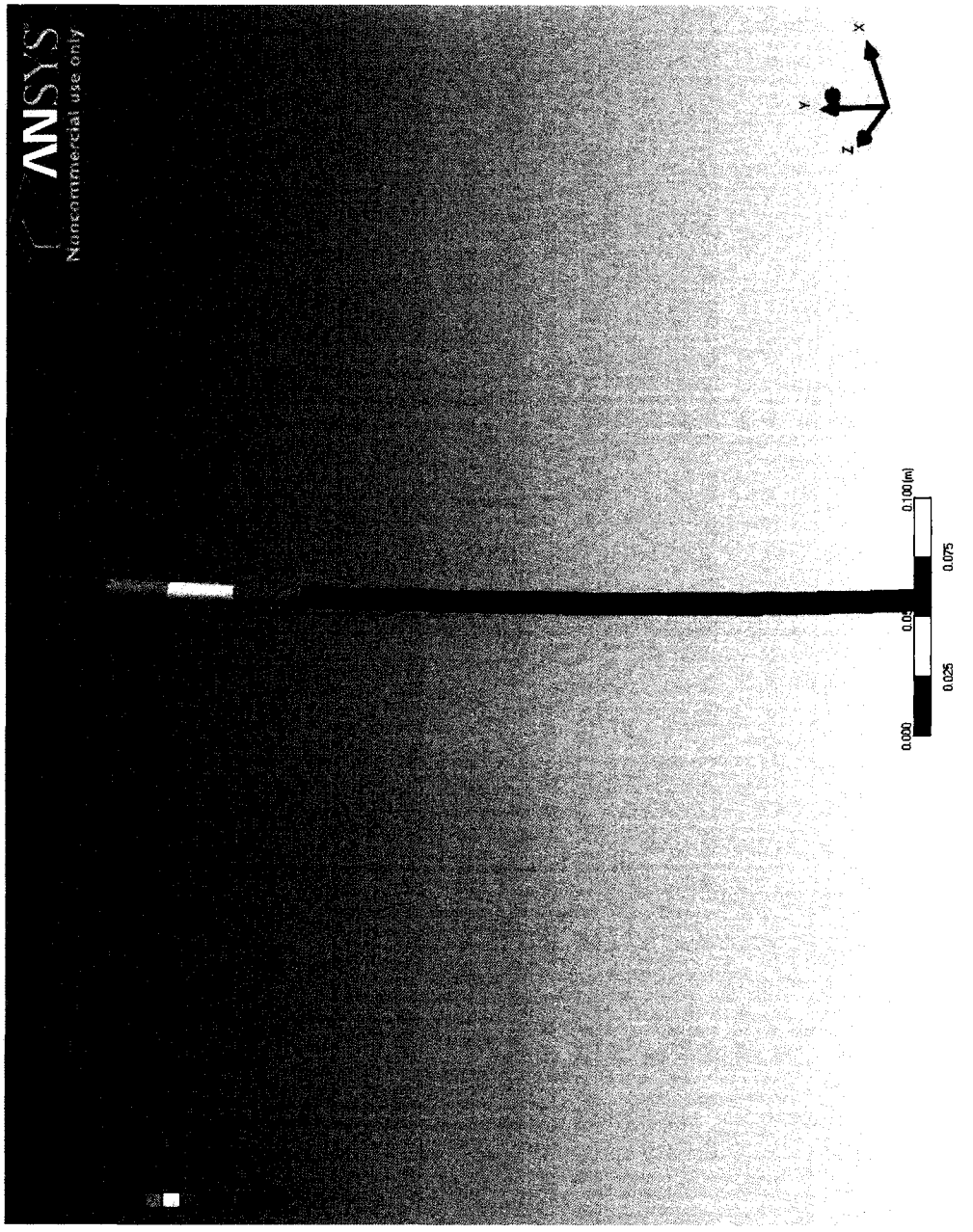

Figure 4.9: ANSYS simulation for the deflection of the inner conductor with a 11″ stainless steel liner, from 1 N applied laterally to the tip.

feedthrough from Insulator Seal [36]. This feedthrough uses a right-cylinder window made from alumina and brazed to a standard 2.75″ stainless steel ConFlat[4] (CF) flange around the outside.

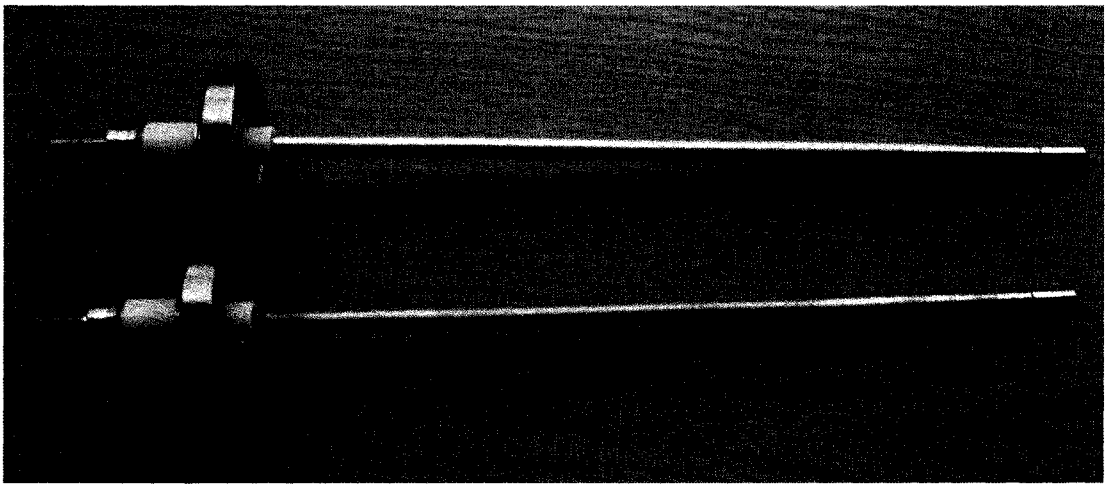

Figure 4.10: RF power vacuum feedthroughs from Insulator Seal. The white portion is the cylindrical alumina window.

Once the first prototype feedthroughs and other components were constructed, an experimental analysis was performed in order to determine the desired inner conductor length. A 40 Hz bandwidth was selected as a goal for amplitude and phase control. Using Equation (3.15), the desired Q_{ext} is 2×10^6. To determine Q_{ext}, a prototype cavity at room temperature was used with a simple probe antenna for the input and the FPC antenna as the pick-up. Because both antennas are very weakly coupled at room temperature, a two coupler method was used to reduce systematic errors. Various tip lengths were attached to the end of the inner conductor and the external quality factor was measured for three different penetration depths. The measured Q_{ext} values are shown in Figure 4.11. From Figure 4.11, the desired penetration is 0.668″.

[4] ConFlat is a registered trade mark of the Varian Corp.

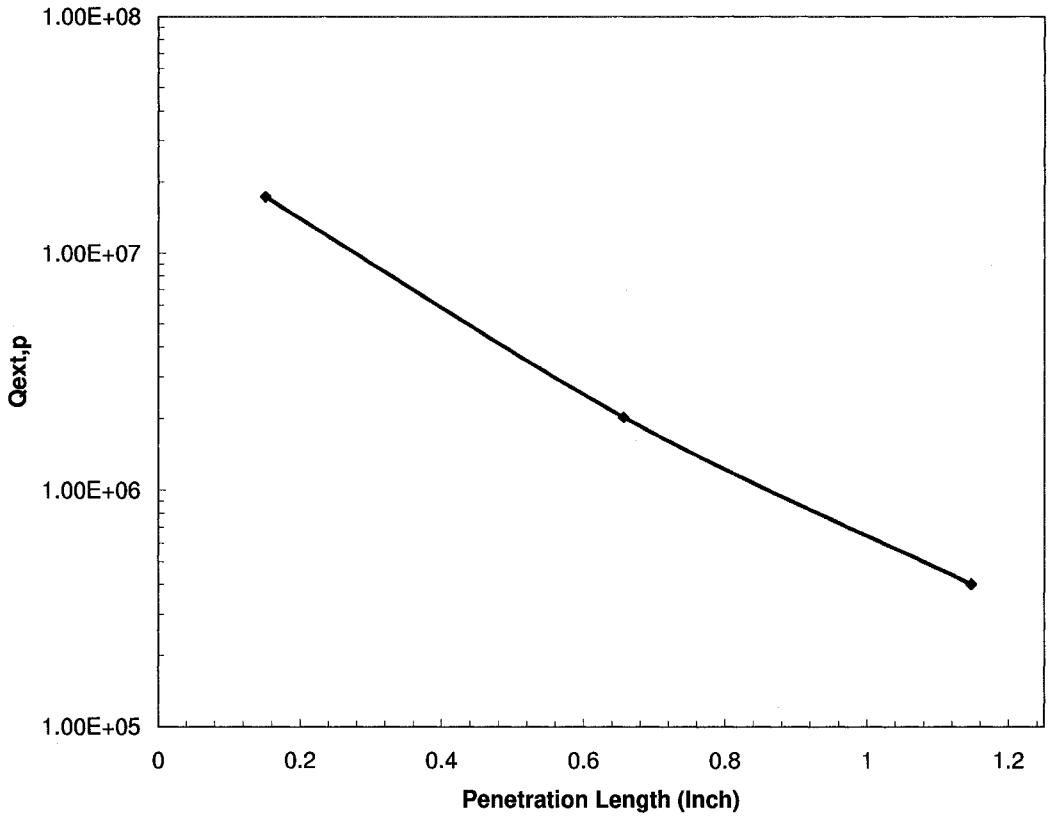

Figure 4.11: Q_{ext} versus coupler penetration length for the 80.5 MHz, $\beta = 0.041$ cavity. The length is measured from the inside of the bottom flange.

4.6 Diagnostics

Section 3.7 described some of the common causes and ramifications of a coupler failure. This section will provide the methods and devices that were used to reduce the risk of failure. The FPC presented here was designed with three diagnostic ports located on the vacuum side outer conductor, close to the window. These three ports house the instruments used to monitor the condition of the alumina window. The sensors mounted here are a cold cathode gauge (Series 903, I-Mag[5]), spark detector, and a current probe.

If multipacting were to occur at the window, there would be a reduction in transmitted power, along with a sharp increase in pressure. The probe may detect the current from the cascading electrons, while the vacuum gauge would measure the change in vacuum. These two diagnostics will be used to detect multipacting and prevent heating or breakage of the window. If multipacting is detected, the input power level or duty cycle can be reduced in order to condition the multipacting barriers. This is useful during conditioning of the coupler, but is undesirable during operation. In addition to these two diagnostics, the coupler also has a sapphire window for spark detection. A photodiode is used to detect any light emissions resulting from multipacting, field emissions, or other breakdown phenomena.

Heating of the conductors can be problematic as well. As discussed earlier, the coupler will employ copper plating in the outer conductor to reduce RF heating. However the plating itself could become an issue. Precise plating procedures must be adhered to in order to provide proper copper adhesion, thickness, and surface finish. The plating must survive ultrasonic cleaning and high temperature baking. Proper care must be taken at all points in the assembly to prevent damage to the copper layer. If the plating does not adhere properly, it could reduce the coupler performance, or produce a cleanliness problem.

[5] A product of MKS Instruments, Inc., Andover, Massachusetts.

Aside from transmission faults, preventive measures are also taken to avoid vacuum faults. The ceramic window is weakest part to the coupler. In addition to being robust enough to withstand the requirements of operation, the window must also be able to survive the coupler assembly. Small fractures or other damage can occur while the cryomodule is being assembled, and may go unnoticed until after the module is completed. In an effort to reduce the probability of this happening, the air-side portion of the coupler was designed to be as unobtrusive as possible. The outside components are attached after the assembly of the module has been completed. Part of the design includes a spacer ring between the air-side outer conductor and the feedthrough flange. This spacing ring will transfer forces from the outer conductor to the flange instead of the ceramic. In the event over-tightening of the assembly occurs, the stresses will not be applied to the braze joints or window.

Precautions can be taken to reduce the chances of a vacuum incident, however if a vacuum breach were to occur, steps have also been taken to detect and minimize the resulting damage. The air-side RF connection of the FPC utilizes a sealed N-type adapter from Myat[6]. This adapter comes with a gas port which will allow the air-side portion of the FPC to be filled with argon gas. If a window rupture or braze failure were to occur, only the clean argon will enter the cavity vacuum. This will prevent the dirty outside air from contaminating the QWR. There will also be a residual gas analyzer (RGA) monitoring the status of the vacuum and it will be able to detect an increase in argon content due to small leaks, allowing for corrective measures to be taken before a catastrophic failure.

The modules used for ReA3 also have separate cavity vacuum and insulation vacuum [7]. In the event of a leak in the coupler bellows, the insulation vacuum would be compromised, but the cavity vacuum would not be affected and thus reprocessing of the cavities would not be required.

Although these measures can be used to reduce the risk of a coupler failure, there is

[6] Myat, Inc., Mahwah, New Jersey.

no guarantee that a problem won't occur. Proper assembly and handling procedures must be observed during the entire assembly process to reduce the chance of a fault.

Chapter 5

Coupler Cleaning, Conditioning and Testing

Four complete prototype coupler assemblies have been manufactured. This chapter will discuss the methods used to test the performance of two of these FPCs. Section 5.1 explains how the windows and vacuum-side components were inspected, cleaned, and assembled for processing. After the two-coupler assembly was built, the fixture was baked to drive out water and residual gases as described in Section 5.2. Conditioning of the couplers was done using a standing-wave method discussed in Section 5.3. Section 5.4 shows the results of high power traveling wave testing of the couplers after conditioning. Finally, Section 5.5 will go over issues encountered during the assembly and conditioning, and explain the steps taken to avoid future mishaps.

5.1 Coupler Preparation and Cleaning

The first step in preparing the couplers for assembly was to inspect all of the coupler components. It was especially important to check the dimensions and visually inspect the condition of the braze joints and ceramic window of the feedthrough. Once the inner conductor length was verified, the properly sized tip was soldered into place and

vacuum tested. If there was an issue with the vacuum integrity, the leak check would identify the problem before the cleaning and assembly of the components. The leak check found no issues with any of the four prototype feedthroughs. The couplers share the cavity vacuum, therefore every part on the vacuum side was wiped down with acetone first, then methanol, before being transferred into a class 10,000 clean room. Once inside the clean room, the pieces were ultrasonically cleaned for 20 minutes using a degreasing solution (Micro-90[1]) solution, and then ultrasonically rinsed for 40 minutes in ultra pure water. Due to the fragility of the windows, the feedthroughs were cleaned for only 15 minutes in a weaker concentration solution before rinsing for an additional 20 minutes. All the pieces were then left to air dry in the clean room for 24 hours.

It is common to process couplers in pairs, usually connected by a waveguide or cavity [13]. Because of the low operating frequency, neither of these approaches was practical. The method that was used in this case was to electrically connect the two inner conductors together with a copper barrel and condition them both simultaneously, as shown in Figure A.5. The coupler components were assembled as shown in Figure 5.1, following the procedure outlined in Appendix B. All fasteners were double-checked to ensure a proper vacuum seal on all flanges. The entire apparatus was then connected to both a scroll pump and a turbomolecular pump, before being leak checked using helium gas and the RGA. Once the vacuum integrity was verified, and the pressure was better than 1×10^{-7} torr, the valves were closed and the scroll pump disconnected, allowing the entire assembly to be transferred to the conditioning area.

[1] A product of Cole-Parmer, Vernon Hills, Illinois.

Figure 5.1: Assembly of the power coupler test fixture inside a class 10,000 clean room.

5.2 Bake-out

The assembled FPCs were reconnected to the vacuum pumps and then subjected to a bake-out. Heat was applied to the couplers in order to drive out water from the metal and ceramic surfaces inside the vacuum assembly. The water was evaporated by the heat and then the gaseous matter was removed from the system by the vacuum pumps. The method used was rather rudimentary: the portion of the coupler assembly under vacuum was wrapped in heat tape. Thermocouples were placed along the outer conductors, and inside the inner conductors, as shown in Figure 5.2. Then the entire apparatus was wrapped with aluminum foil to retain the heat and minimize temperature fluctuations, as shown in Figure 5.3. Heat was then applied using two feedback-controlled thermal regulators (Omega CSC32[2]), which monitor and maintain a steady temperature, while the temperature and vacuum levels were monitored by a Windows PC running LabVIEW[3]. The heat was applied only to the outer conductors and was approximately 175° C, this radiantly heated the inner conductors to temperatures exceeding 100° C. The temperature was hot enough to evaporate any water trapped inside the fixture. The heat was applied for 36 hours, until the vacuum pressure no longer showed much improvement. As can be seen in 5.4, the outer conductor temperatures overshot to 195° C and then settled to 175° C after about 3 hours. The pressure rose to 3×10^{-5} torr as the temperatures ramped up, and then gradually fell, reaching 1×10^{-6} torr by the end of the bake-out. The pressure dropped rapidly after the heaters were turned off. The temperature spikes near the three hour mark was the result of running an "auto-tune" function on the temperature controllers to reduce temperature fluctuations.

It is important to ensure that the entire coupler assembly is capable of withstanding the elevated temperatures of baking. The MKS cold cathode vacuum gauges can be baked at temperatures up to 500° C without the plastic exterior magnet assembly.

[2] A product of Omega Engineering, Inc., Stamford, Connecticut.
[3] A product of National Instruments, Austin, Texas.

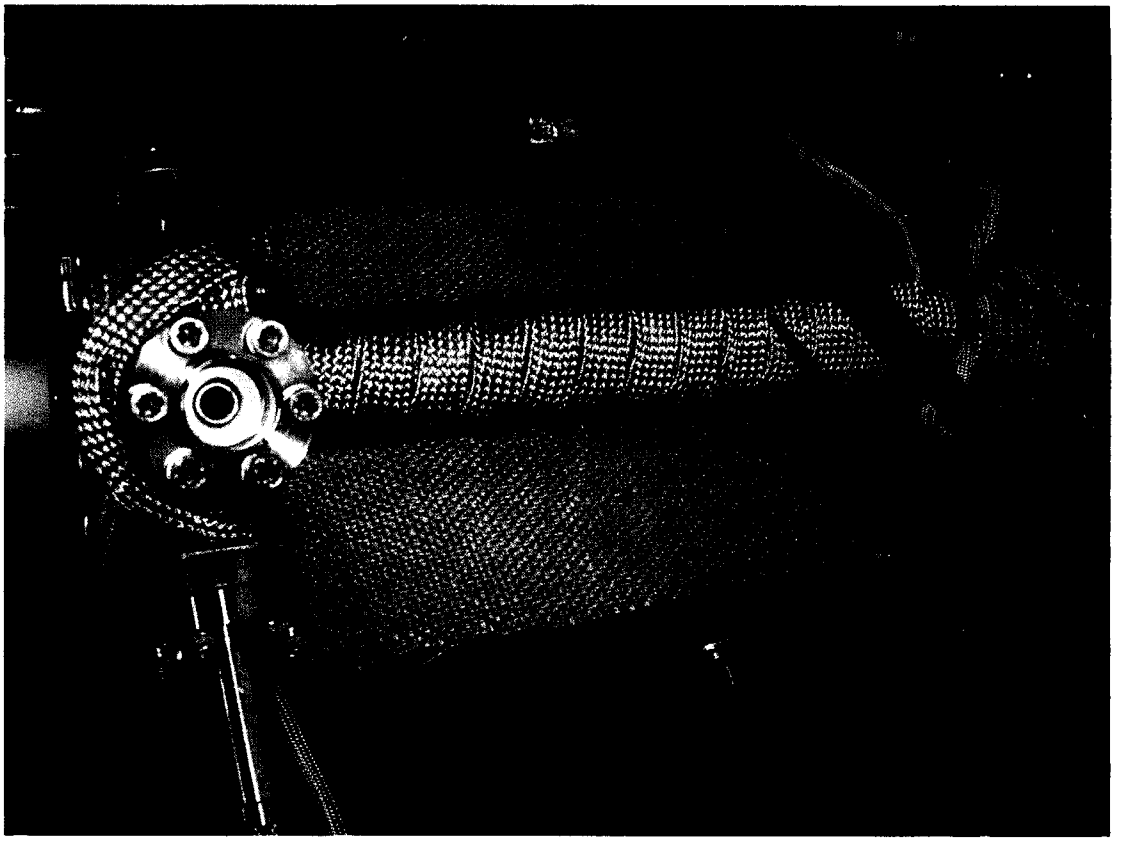

Figure 5.2: Outer conductor of a power coupler wrapped in heat tape prior to bake-out. The ceramic window is visible on the left.

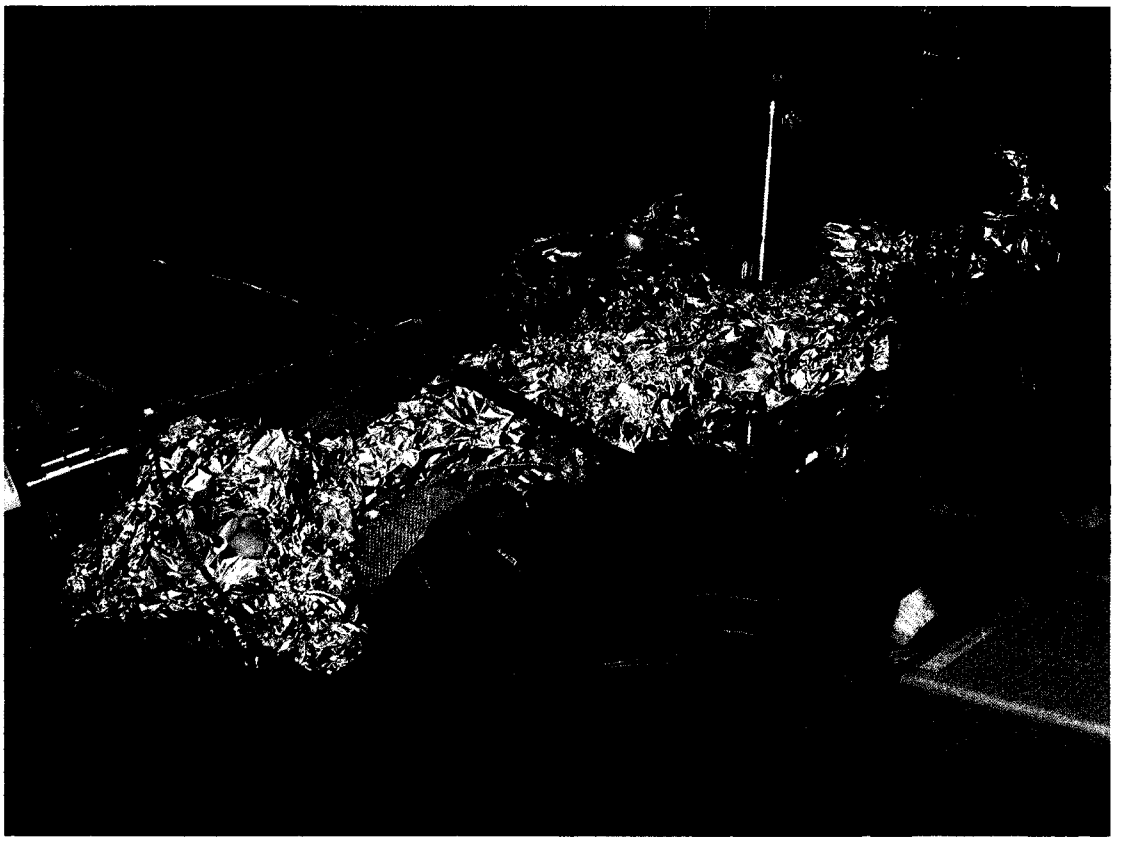

Figure 5.3: Power coupler conditioning fixture wrapped in foil for baking.

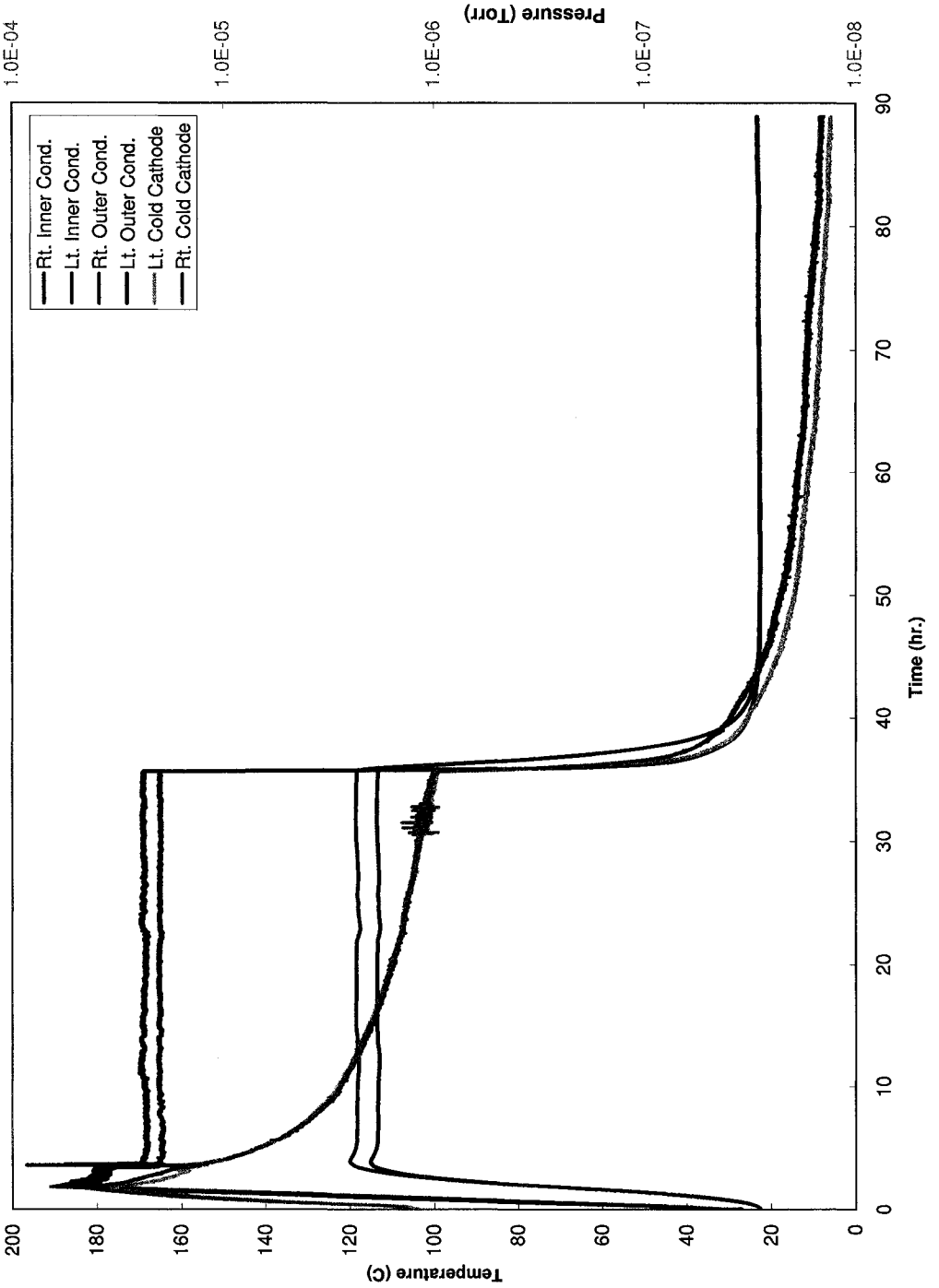

Figure 5.4: Temperature and pressure measurements taken during the bake-out. The vacuum pressure on plotted along the right vertical axis.

The manufacturer recommended temperatures of less than 150° C at the mounting flange with the magnet assembly in place. This temperature was monitored in order to allow continuous pressure logging while baking. The temperature at the flange did not exceed 40° C at any point in the process. The electron multiplier of the RGA cannot be operated at temperatures exceeding 50° C, but can be heated to 250° C if the filament is not energized. This meant we were unable to monitor the residual gas levels during the bake.

Prior to baking, the gas levels recorded, as shown in Figure 5.5. The bar graph on right indicate the levels of the gases present, and the line plot on the left is the partial pressure as a function of time for some of the gases. The numbers on the RGA bar graph correspond to the atomic mass of the gas being measured. Some masses of interest are 2 for hydrogen, 4 for helium, 18 for water, 14 and 28 for nitrogen gas, 40 for argon, and 44 for carbon dioxide.

After 36 hours of baking, the power to the heat tape was turned off, and the system was allowed to cool. The foil was left in place during this time. Two hours after the heat was turned off, when the temperatures had dropped to a safe level, the RGA was turned back on and levels were again recorded, as seen in Figure 5.6. The levels of all the major gases showed a marked increase. The system was then allowed to sit for 48 hours to allow the residual gases to be pumped from the system. A dramatic reduction of residual gases was seen after 48 hours, as shown in Figure 5.7. The assembly was now ready for conditioning. More information on the baking procedure can be found in Appendix C.

5.3 Coupler Conditioning

The coupler conditioning fixture was assembled with 1 5/8″ EIA to N-type sealed adapters at each end, and the ports were connected to a calibrated VNA. The transmission and reflection coefficients were measured and compared to the previously

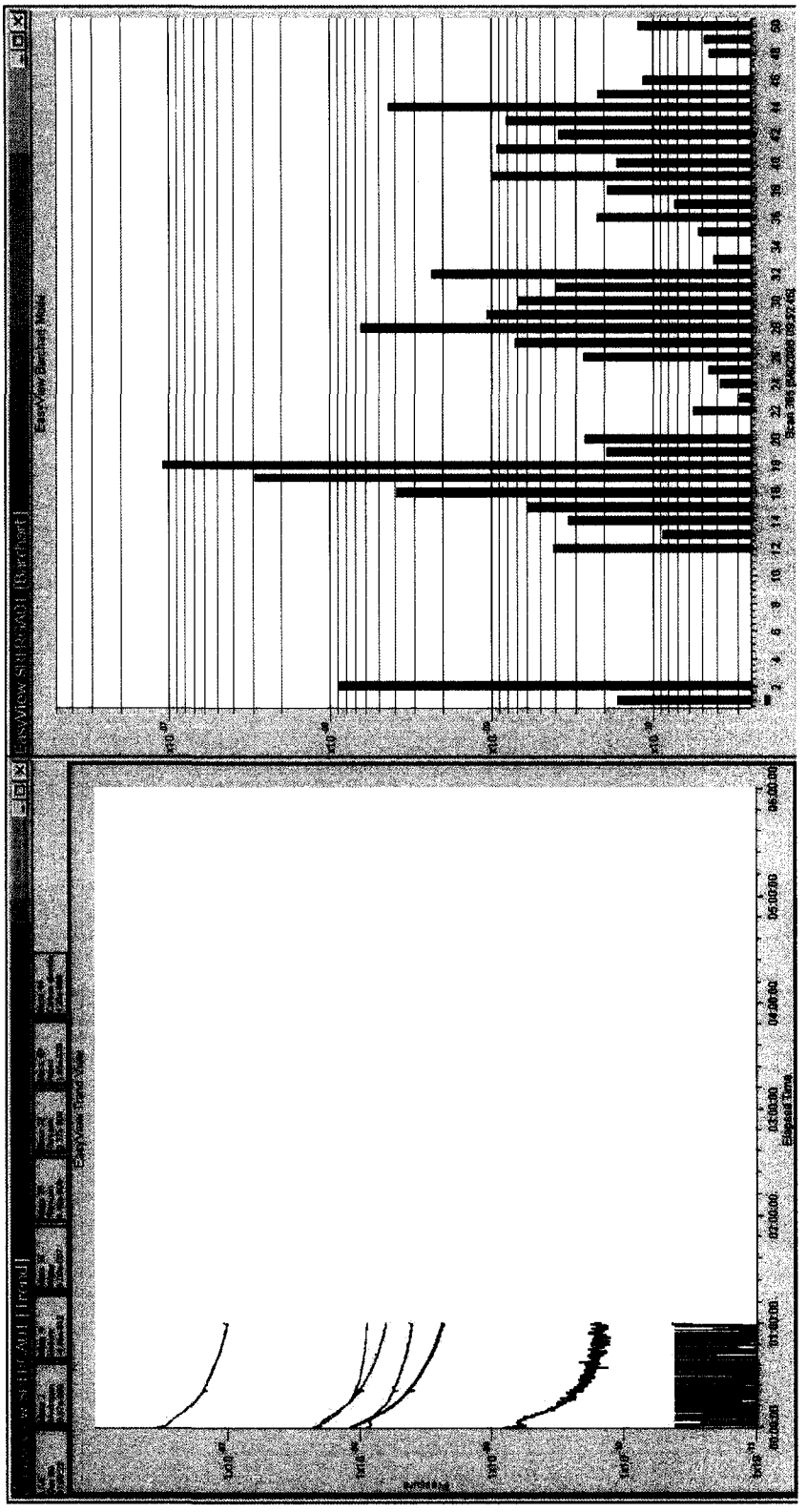

Figure 5.5: Residual gases in the conditioning assembly prior to baking out.

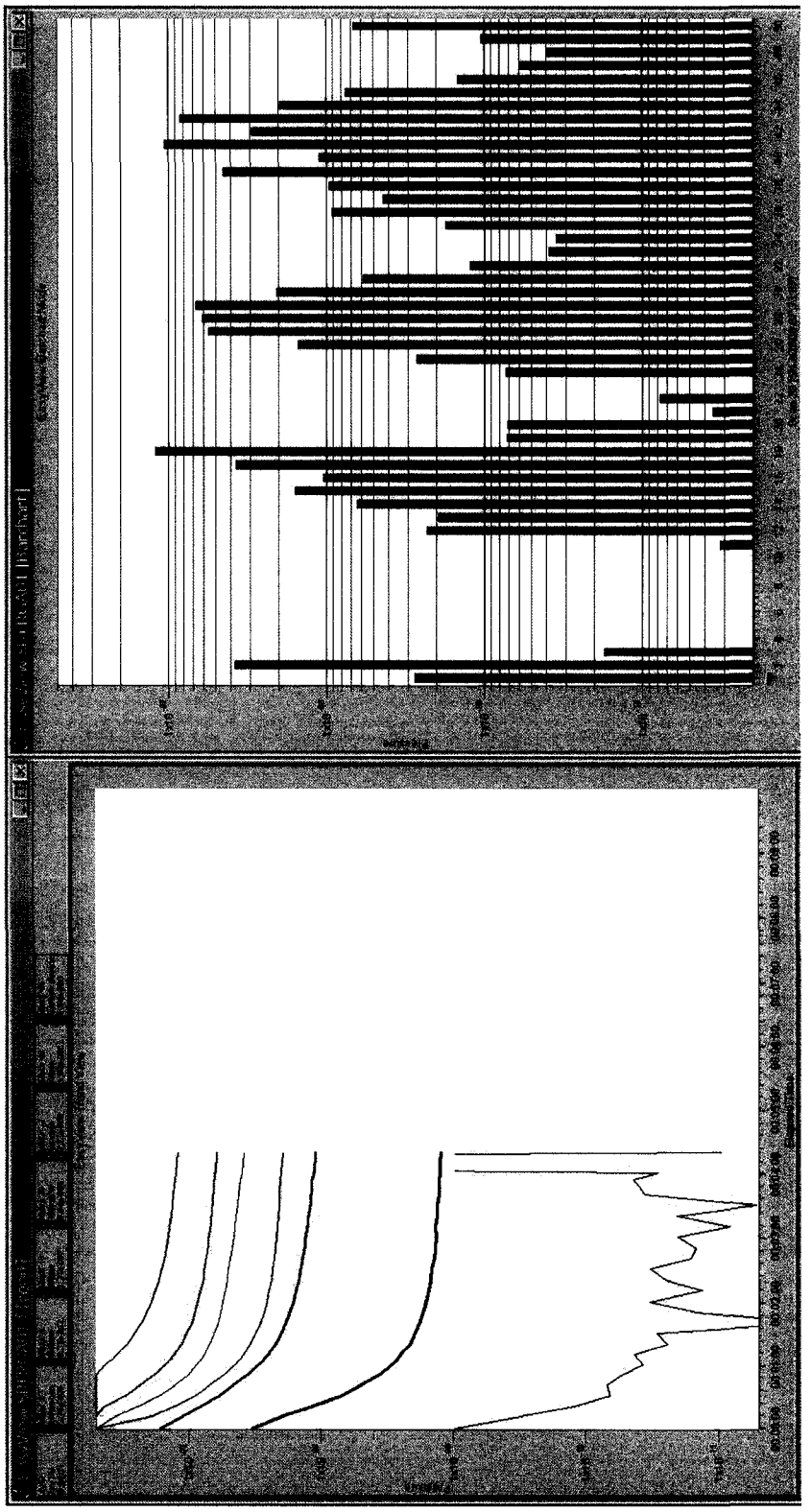

Figure 5.6: Increased gases in the fixture 2 hours after baking.

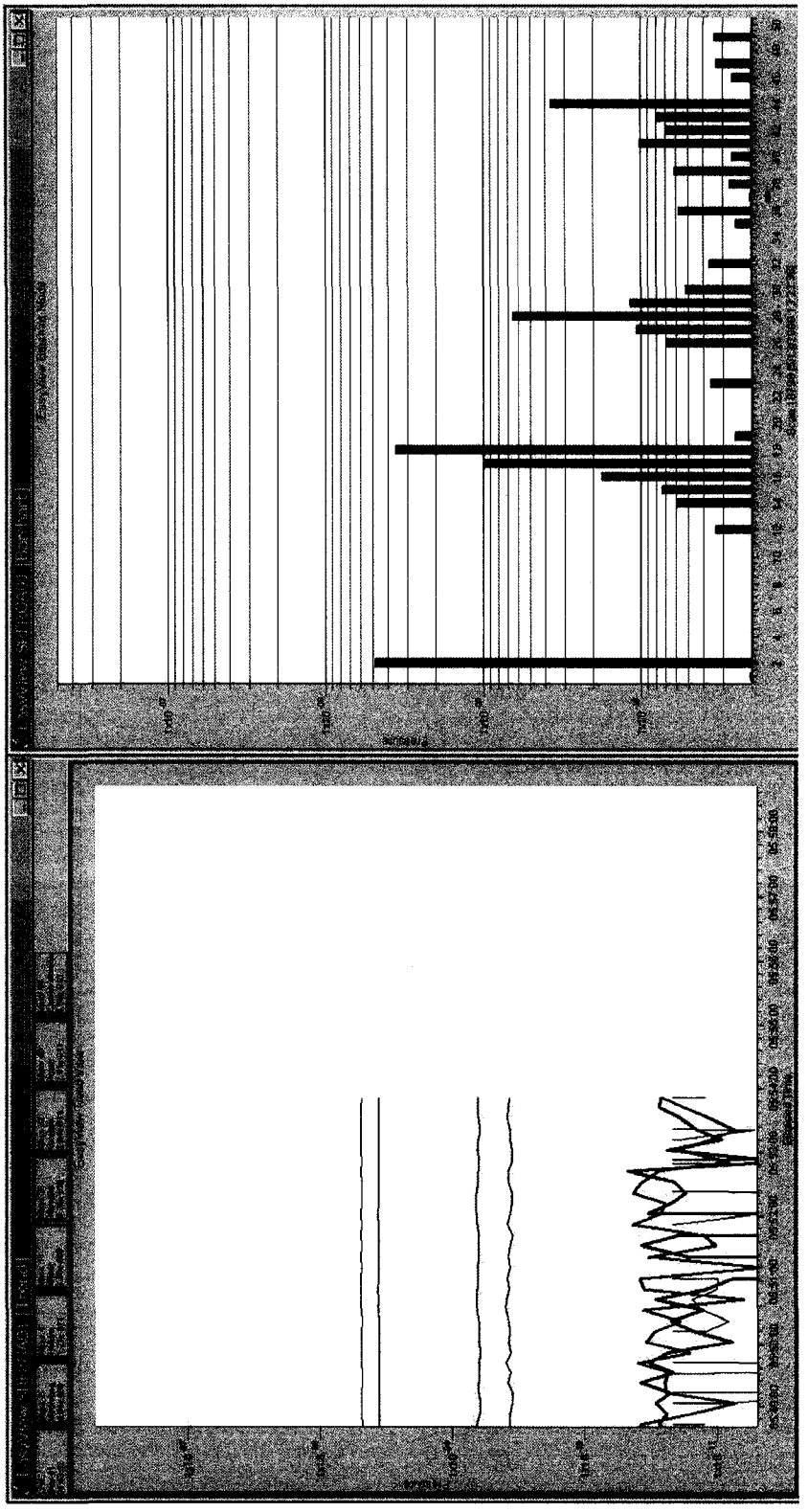

Figure 5.7: Remaining gases after pumping on fixture for 24 hours after baking.

simulated results. The results of the reflection and transmission measurements are provided in Figures 5.8 and 5.9 respectively. At 80.5 MHz, the measured reflection coefficient was -26 dB and the measured transmission coefficient was -0.02 dB. The experimental results can be expected to differ from the simulations because the measured values were continuous and included the connectors, while the simulations were for only the RF windows only and do not account for connection losses.

Prior to starting the conditioning, it was necessary to perform a system calibration in order to obtain accurate power measurements. The power coupler conditioning setup was connected to the electronic equipment as shown in Figure 5.10. Calibrations were performed in order to calculate the actual traveling wave power levels from the power signals measured using directional couplers and power meters. See Appendix C for details.

Initially the power was applied in traveling wave mode. The power was increased while monitoring the pressure and transmitted power. This was done to check the assembly for any transmission issues before conditioning. Next, the sliding shorts were connected to the coupler assembly for conditioning in standing wave mode, as shown in Figure 5.11. Using a standing-wave method of conditioning turns the test fixture into a resonant cavity that can be easily tuned to the desired frequency. The equivalent power in the standing wave was found to be

$$P_{sw} = P_f + 20\ dB \tag{5.1}$$

by using a 1 5/8″ EIA bi-directional coupler and comparing the values for the traveling wave to the standing wave mode. This allows the couplers to be conditioned at powers greater than the RF amplifier can supply alone. Using this method we were able to condition the couplers at 10 kW, much greater than the maximum power that they will experience during normal operation.

The sliding shorts were placed a full wavelength apart at 80.5 MHz. The ends of

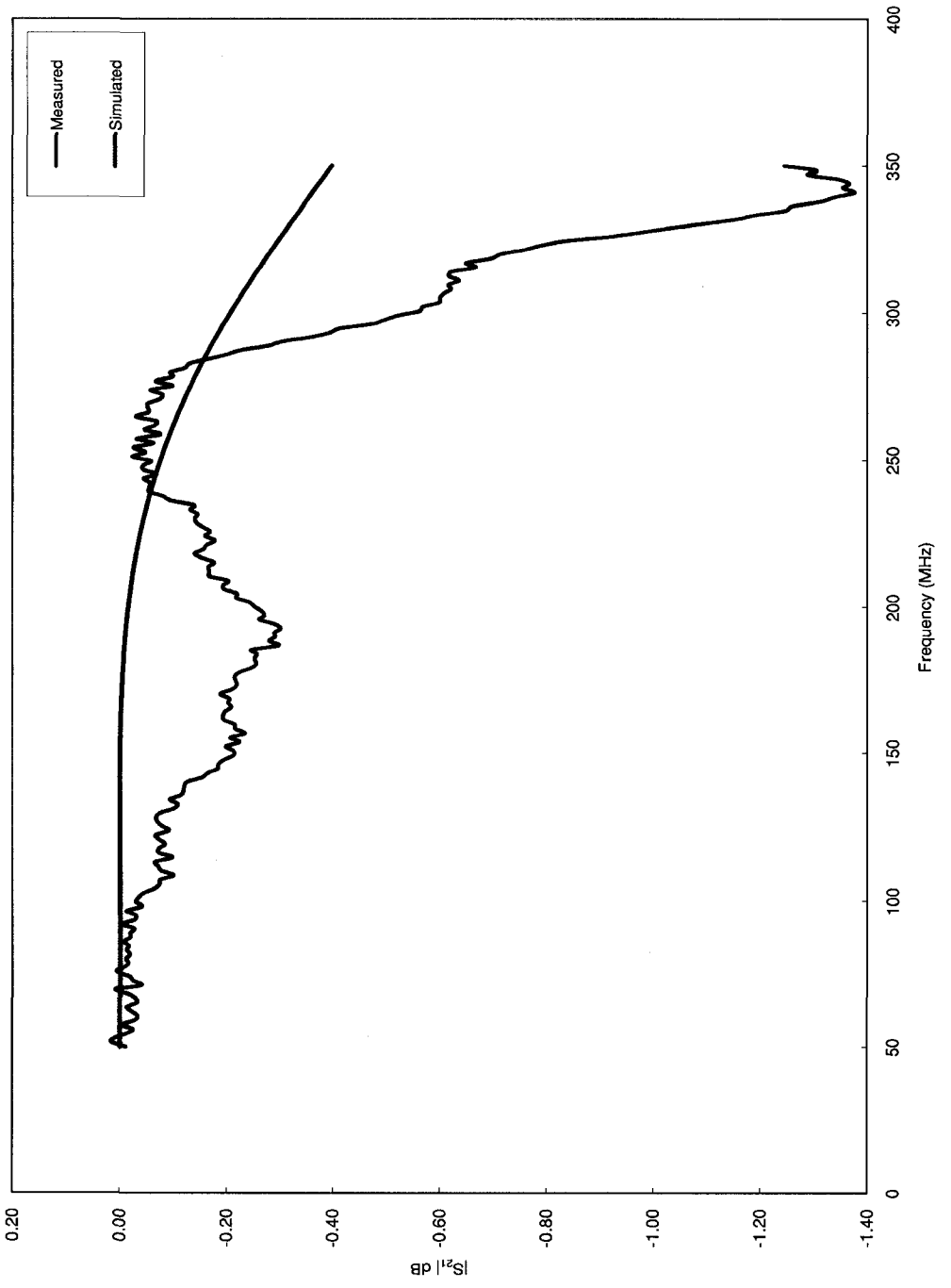

Figure 5.8: The measured and simulated transmission coefficients through the two-coupler assembly.

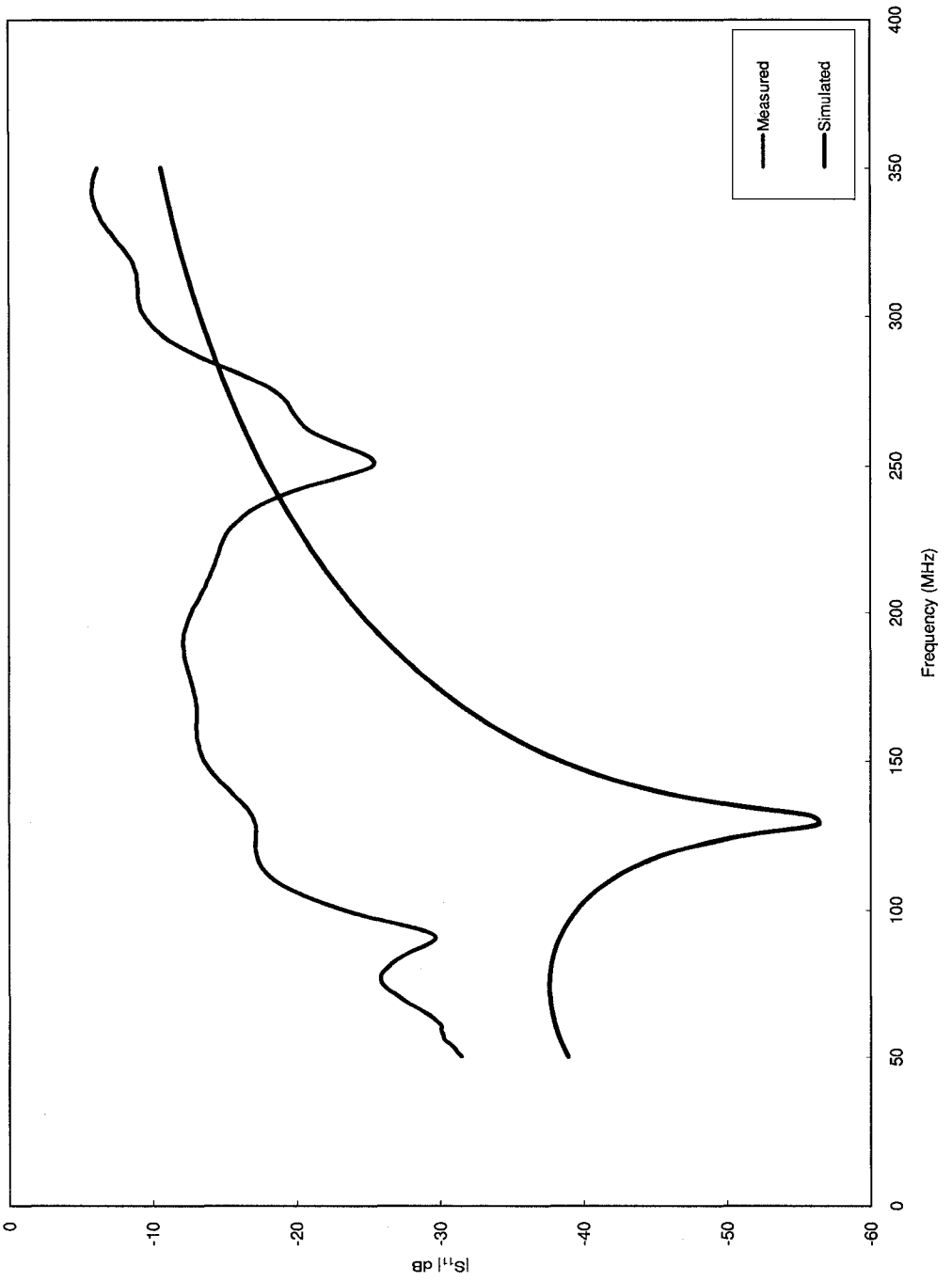

Figure 5.9: The measured and simulated transmission coefficients through the two-coupler assembly.

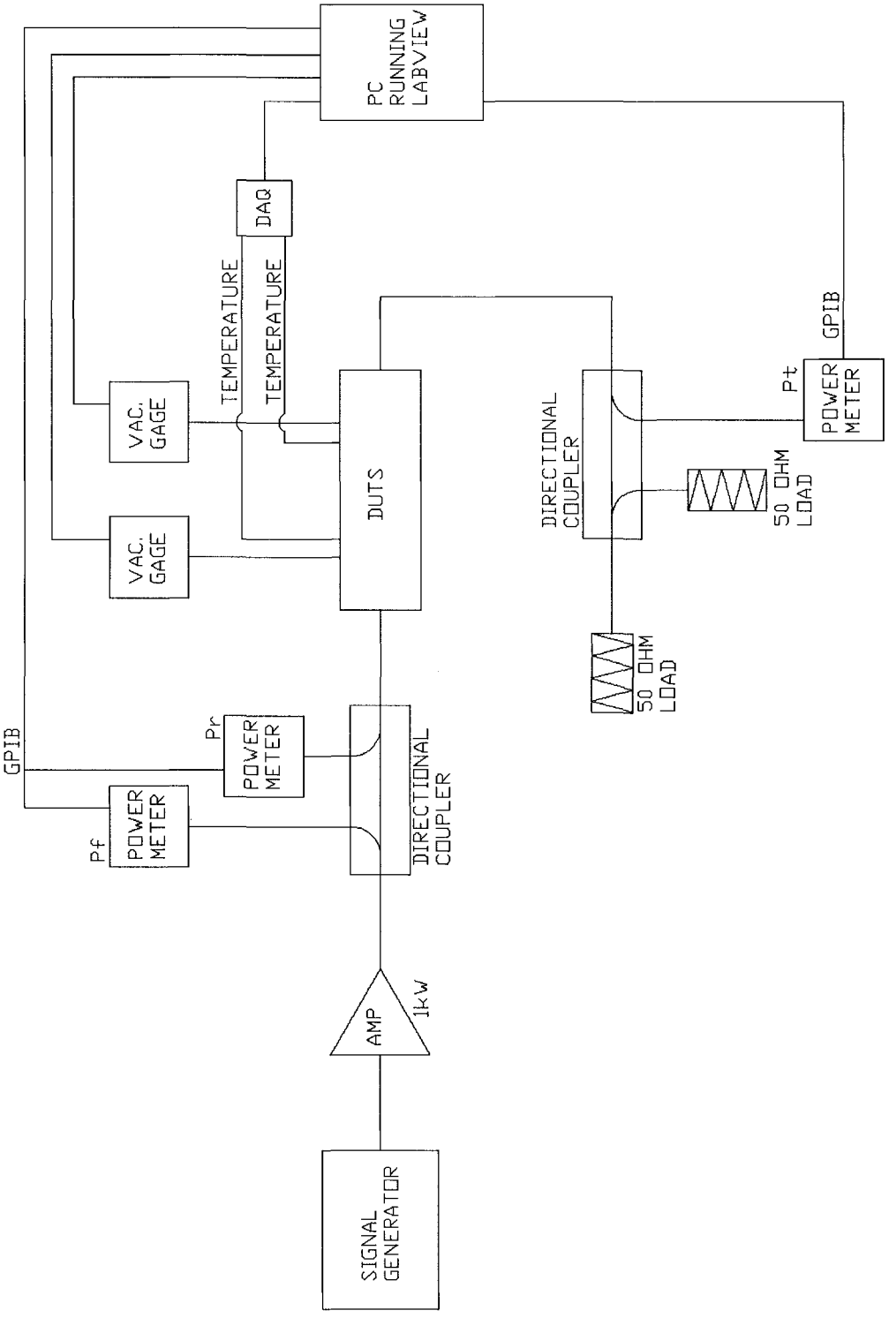

Figure 5.10: Schematic diagram of the power coupler conditioning system.

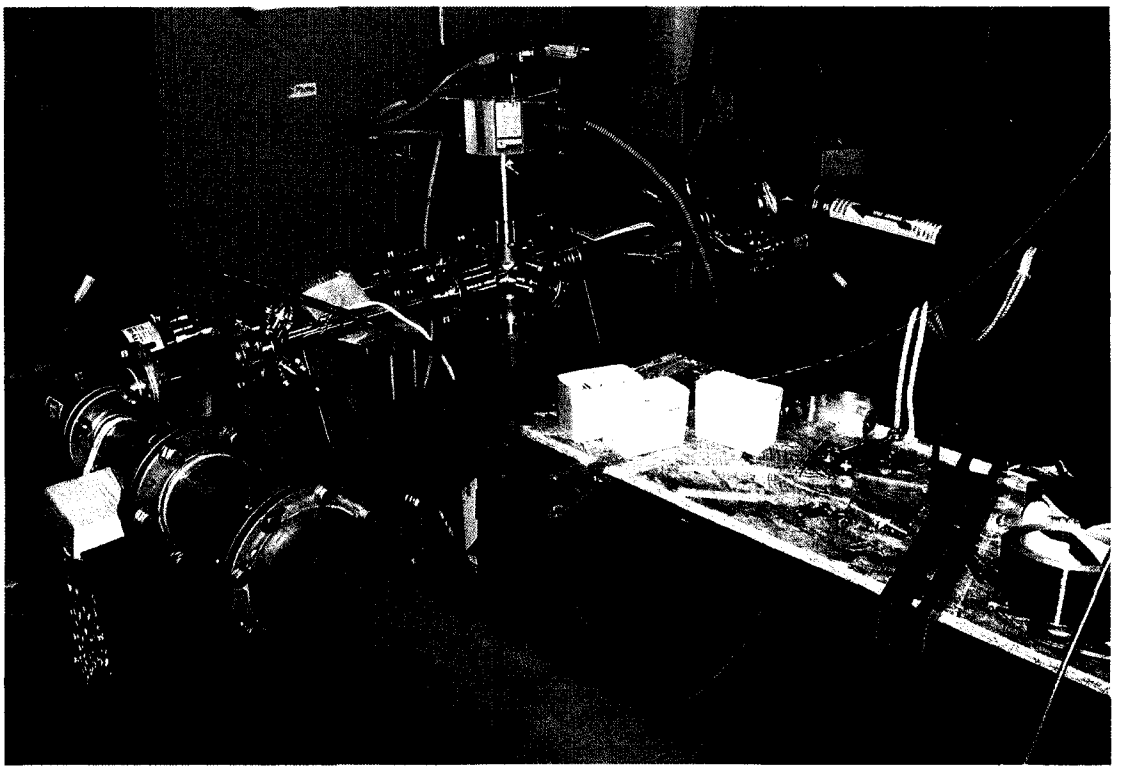

Figure 5.11: The sliding short assembly as installed for conditioning in standing wave mode. The large diameter pipe in the foreground is the input side, and the small diameter one near the upper-right corner was used to adjust the resonant frequency.

the shorts were located at current maxima and voltage minima. This allowed either coupler window to be subjected to both voltage and current maxima by moving both shorts by equal amounts. During conditioning, the position of the peaks were swept across the entire length of both couplers. The shorts were moved 24 times in 3″ increments in order to cover the entire length of the coupler assembly. The patterns of the standing wave voltage and currents used to condition are shown in Figures 5.12 and 5.13 respectively.

The conditioning was relatively simple, starting with the smaller diameter short completely inserted. The large diameter short was then positioned so that the assembly resonated at 80.5 MHz. Power was then applied to the structure, and slowly ramped up until the standing-wave power reached 70 dBm, while the pressure inside the fixture was closely monitored. It is recommended to not allow the pressure inside the assembly to increase above 10^{-7} torr in order to prevent damage to the windows [13, 15, 37].

During conditioning, some short positions did not produce any increase in pressure and were conditioned for approximately 15 minutes. Other short positions, such as near the windows produced large pressure increases, and required heavy conditioning. As the pressure began to approach the safe limit, the input power was set to slowly pulse. When the vacuum began to recover, the pulse length was slowly increased until the input power was again at CW. A more detailed description of the conditioning procedure is provided in Appendix C.

The problematic short positions were the result of materials embedded in the windows and multipacting. The multipacting also caused an increase in the outer conductor temperatures. Conditioning the problem areas created a substantial increase in the gases measured by the RGA. Compared to Figure 5.7, which was prior to starting the conditioning, Figure 5.14 shows the increased levels caused by the conditioning of a vacuum window. As the vacuum recovered and the contaminants

were removed, the residual gases were depleted, as shown in Figure 5.15.

After conditioning in standing wave mode, the assembly was tested with standing-wave power equivalent to 10 kW, much greater than what is necessary for normal operation. Some multipacting was observed near the ceramic windows, but these barriers were easily conditioned away by pulsing the input power as necessary.

5.4 High Power Testing

After completing the conditioning of the couplers, a long-term durability test of the couplers was performed. In order to do this, the sliding shorts were removed and the N-type adapters were reinstalled. One end of the coupler assembly was connected to the amplifier through a directional coupler. The other end was connected to a 1 kW, oil-filled matched load. The input power was steadily increased until 500 W of forward power was applied to the system and measured. At this point the directional coupler was removed because it was rated for only 500 W. Power was reapplied to the system until the 1 kW limit of the amplifier was reached. The system was left to run at full power for seven days uninterrupted, while the pressure and temperature were continuously monitored. After seven days, the power was turned off and a temperature sensitive label mounted to a stainless steel rod was inserted into an inner conductor. Full power was then reapplied for three hours to measure the temperature of the inner conductor near the tip. The label was removed and the tip temperature was noted as reaching 49° C. This process was then repeated with a new label, and the test was repeated for 24 hours. The internal temperature peaked at 54° C this time. The temperature variation was not large, so that the conductive cooling of the inner conductor should be sufficient for operation of the re-accelerator.

One final RGA reading was taken after the endurance test. Figure 5.16 shows that the majority of the residual gases were removed from the system and the vacuum pressure improved to 5.6×10^{-9} torr. The testing of the coupler assembly was

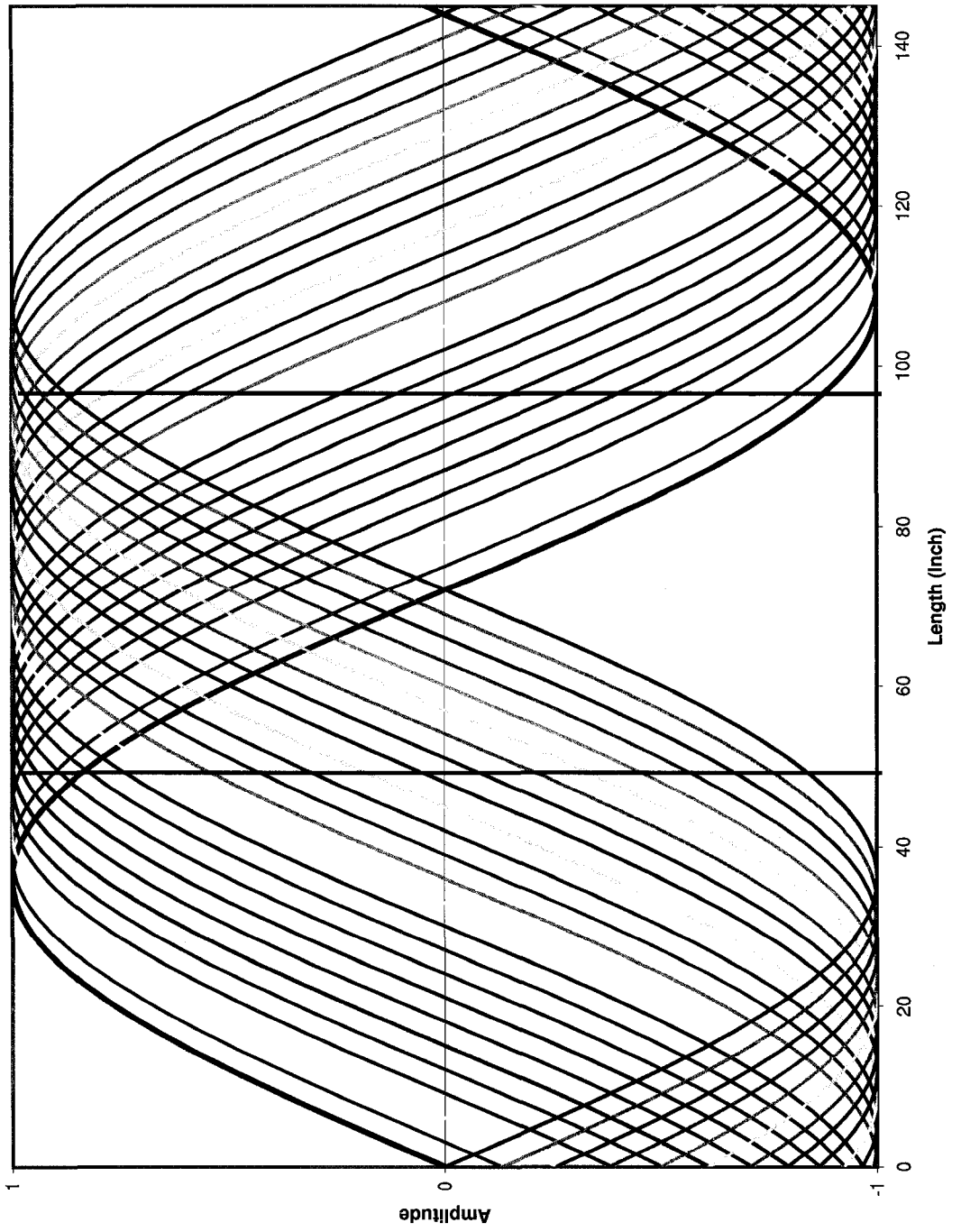

Figure 5.12: Standing wave voltage sweep pattern. The vertical black lines are the window locations; the dark blue line is the initial sweep position.

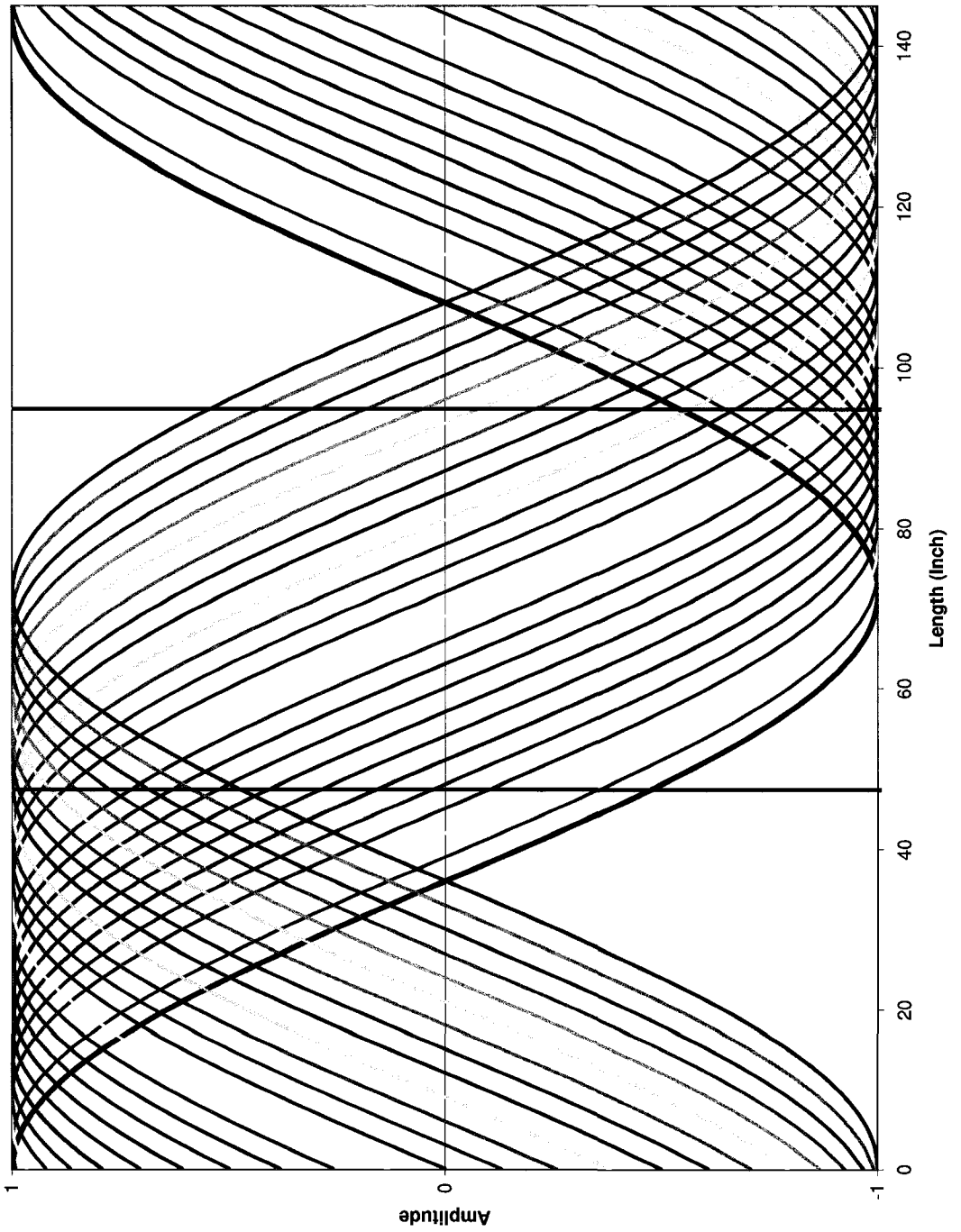

Figure 5.13: Standing wave current sweep pattern. The vertical black lines are the window locations; the dark blue line is the initial sweep position.

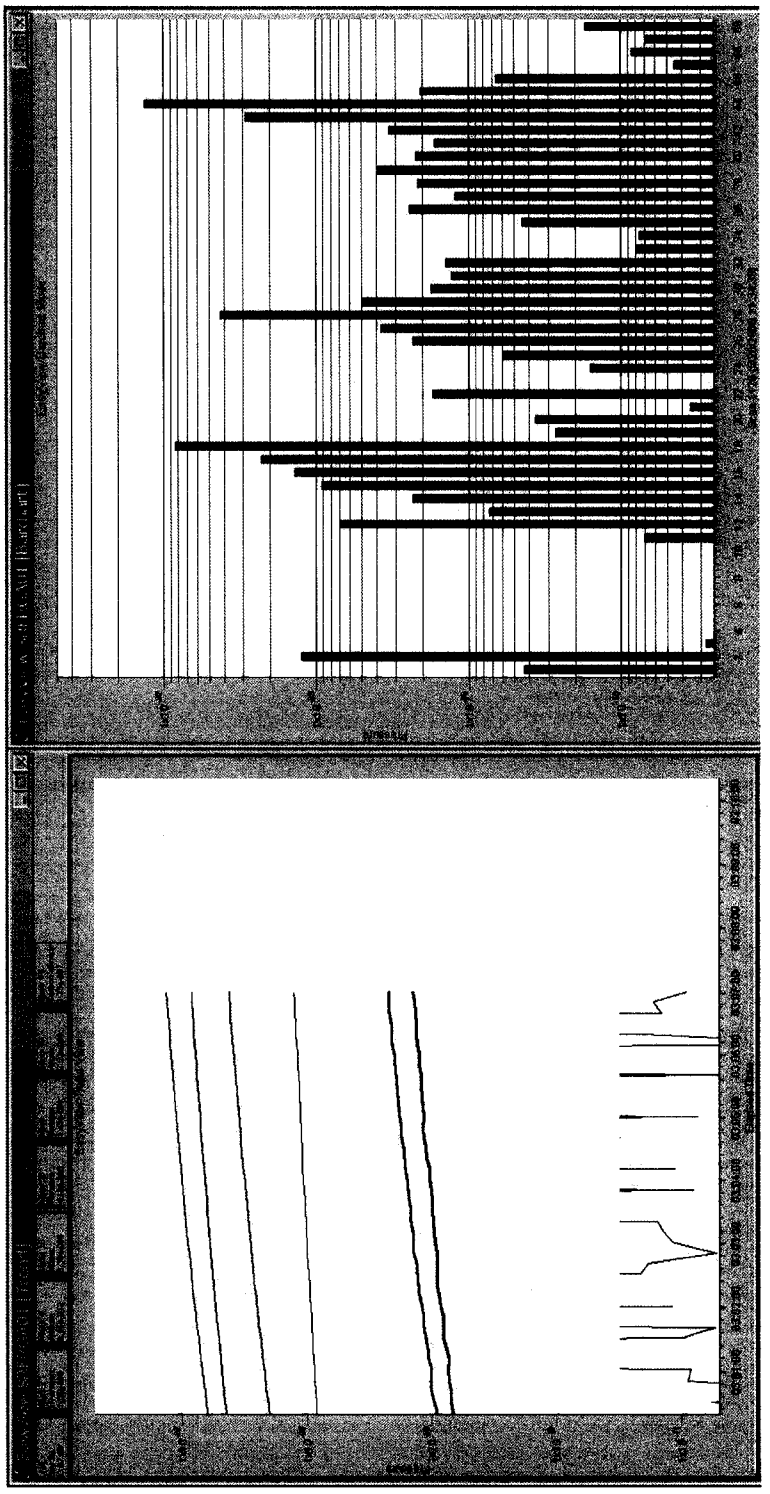

Figure 5.14: Increased RGA reading resulting from conditioning a "dirty" area of the power coupler assembly. Note the increasing trend indicating gas levels are still climbing.